A universal filter for enhanced imaging with small arrays

Liliana Borcea[1], Thomas Callaghan[2], Josselin Garnier[3], and George Papanicolaou[4]

[1] Computational and Applied Mathematics, MS134, Rice University, 6100 Main Street, Houston, TX 77005-1892

[2] Institute for Computational Mathematics in Engineering, Stanford University, Stanford, CA 94305

[3] Laboratoire de Probabilités et Modèles Aléatoires & Laboratoire Jacques-Louis Lions, Université Paris VII, 2 Place Jussieu, 75251 Paris Cedex 5, France

[4] Mathematics Department, Stanford University, Stanford, CA 94305

E-mail: borcea@caam.rice.edu, tscallag@stanford.edu, garnier@math.jussieu.fr, papanico@math.stanford.edu

Abstract. We analyze in detail directivity enhancement in imaging with small arrays of closely spaced sensors, in homogeneous media. Imaging is done with back propagation or migration of the array data after applying an inverse filter that increases the resolution of the image. In general, the construction of such a filter requires invasive measurements on a control array in the vicinity of the object to be imaged, which we assume are not available. The form of the filter is, however, universal if the control array encloses the imaging sensor array. It is the inverse of the finite Fourier transform operator, which has the sinc function as its kernel. We analyze the dependence of resolution enhancement on the signal-to-noise ratio both with narrow and broadband signals.

PACS numbers: 43.60.Pt, 43.60.Gk, 43.60.Tj, 43.60.Cg

Submitted to: *Inverse Problems*

1. Introduction

We analyze in detail enhancement of the cross range resolution, or the directivity, in imaging with small arrays of closely spaced sensors in homogeneous media. Imaging is done with numerical back propagation or migration of the (possibly noisy) array data, both with active and with passive arrays. Active arrays probe the environment with pulses that they emit and then record the echoes from the reflectors to be imaged. Passive arrays record signals from sources which are to be imaged. To enhance the cross range resolution we first apply an inverse filter to the array data and then back propagate them. In general, the construction of such a least squares (LS) filter depends on the matrix of Green's functions from the sensor array to a control array in the vicinity of the object to be imaged. The form of the filter is, however, universal if the control array encloses the imaging sensor array in an appropriate way. It is the inverse of the finite Fourier transform operator, which has the sinc function as its kernel. The purpose of this paper is to analyze the dependence of cross range resolution enhancement on the signal to noise ratio (SNR), both with narrow and broadband signals.

Imaging by numerical back propagation of the array data is the same as travel time or Kirchhoff migration (KM) that is used extensively in seismic imaging [4, 6, 11]. It is also closely related to linearized least squares imaging [4, 8]. The possibility of cross range resolution enhancement was first considered in (narrowband) antenna beamforming [24, 19] and in (broadband) physical time reversal (TR) [23, 22, 13], which is done mainly for wave focusing on signal sources or reflectors [14]. The inverse filter (IF) method is a refinement in which a filter is applied to the time-reversed recorded signals before back propagation [16, 13, 22, 27]. The filter is chosen so that refocusing is enhanced at the target location while energy levels are low at a control array in its vicinity. This is done in a least squares sense using the matrix of Green's functions from the sensor array to the control array. The IF method does enhance cross range resolution, compared to TR or KM, but it is highly invasive since it requires the measurement of the matrix of Green's functions [23, 22, 13]. In [27] it is noted that the inverse filter can be related to a suitably defined backscattering matrix at the sensor array when the control array surrounds it. This allows for a non-invasive implementation of the inverse filter.

In this paper, we specialize to imaging in a homogeneous medium where the inverse filter is the inverse of the finite Fourier transform whose kernel is the sinc function and we analyze the cross range resolution of the image. We use the prolate spheroidal wave functions for this purpose [20, 21]. Resolution in imaging is limited by the SNR of the array data because noise amplification by the inverse filter must be controlled. We analyze in detail the tradeoff between resolution enhancement and noise amplification when using the inverse filter, both for narrow and broadband signals. These are the main results of this paper.

We note that when the inverse filter is used in physical time reversal, or in antenna beamforming, the main limiting factor in enhanced focusing, or directivity, is the

maximal power that the array can deliver. This is different from the SNR limitations of the inverse filter when used in imaging because the back propagation is done numerically.

The paper is organized as follows. In Section 2 we introduce the KM imaging functionals that are used in this paper. In Section 3 we study the optimization problem that determines the least squares (LS) filter and show that the IF method can enhance the resolution of a KM imaging strategy. In Section 4 we show that the LS filter takes a universal form for a large class of control arrays. We show the results of numerical simulations in Section 5. In Sections 6-7 we analyze the performance of the IF method in terms of resolution and SNR when the sensor array is over-sampled (continuous array). We consider the SNR analysis in the context of a discrete array in Section 8 and give an adaptive algorithm for choosing the regularization parameter used in the inverse filter.

2. Migration and inverse filter imaging

2.1. Passive imaging

In imaging with a passive array (Figure 1, left) the object that we want to image is a source or a distribution of sources. The waves propagate in a homogeneous medium and the array sensors at $\{\vec{\mathbf{x}}_r, r = 1, \ldots, N\}$ record the signals $P(\vec{\mathbf{x}}_r, t)$, whose Fourier transforms are:

$$\hat{P}(\vec{\mathbf{x}}_r, \omega) = \int P(\vec{\mathbf{x}}_r, t) e^{i\omega t} dt\,.$$

The goal is to image the spatial distribution of the sources from the array data $(\hat{P}(\vec{\mathbf{x}}_r, \omega))_{r=1,\ldots,N}$. In this paper the background is taken to be homogeneous with velocity c_0.

In passive imaging, Kirchhoff migration (KM) consists in back propagating the recorded signals numerically in a homogeneous medium, which is the same as time reversal when the medium is in fact homogeneous as is assumed here. The back propagated field observed at the search point $\vec{\mathbf{y}}^S$ is the KM imaging functional:

$$\mathcal{I}^{\rm KM}(\vec{\mathbf{y}}^S) = \frac{1}{2\pi} \int d\omega \hat{\mathcal{I}}^{\rm KM}(\vec{\mathbf{y}}^S, \omega)\,, \tag{1}$$

with

$$\hat{\mathcal{I}}^{\rm KM}(\vec{\mathbf{y}}^S, \omega) = \sum_{r=1}^{N} \hat{G}(\vec{\mathbf{y}}^S, \vec{\mathbf{x}}_r, \omega) \overline{\hat{P}(\vec{\mathbf{x}}_r, \omega)}\,. \tag{2}$$

Here $\hat{G}$ is the time-harmonic Green's function in a homogeneous medium given by

$$\hat{G}(\vec{\mathbf{x}}, \vec{\mathbf{y}}, \omega) = \frac{e^{i\frac{\omega}{c_0}|\vec{\mathbf{y}} - \vec{\mathbf{x}}|}}{4\pi|\vec{\mathbf{y}} - \vec{\mathbf{x}}|} \tag{3}$$

in a three-dimensional space, and by

$$\hat{G}(\vec{\mathbf{x}}, \vec{\mathbf{y}}, \omega) = \frac{i}{4} H_0^{(1)}\Big(\frac{\omega}{c_0}|\vec{\mathbf{y}} - \vec{\mathbf{x}}|\Big) \tag{4}$$

in a two-dimensional space.

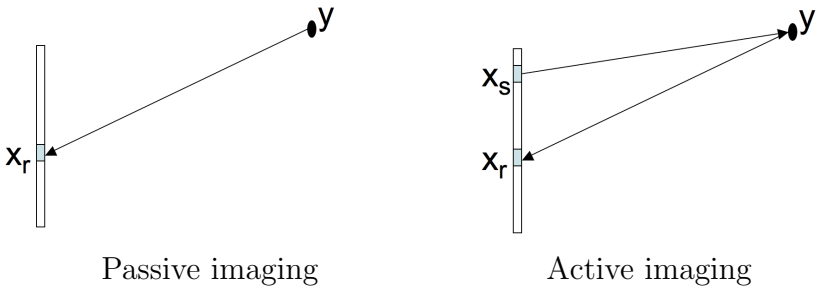

Figure 1. Left: A passive imaging configuration in which the object to be imaged is a point source at $\vec{\mathbf{y}}$ and the array sensors at $\vec{\mathbf{x}}_r$ $(r = 1, \ldots, N)$ record the signals emitted by this source. Right: An active imaging configuration in which the object to be imaged is a small reflector at $\vec{\mathbf{y}}$, and the array sensors at $\vec{\mathbf{x}}_s$, $s = 1, \ldots, N$, emit probing pulses. The back scattered signals are recorded at the array sensors located at $\vec{\mathbf{x}}_r$, $r = 1, \ldots, N$. Here the same array is used for illumination and recording.

If a filter $(\hat{K}(\vec{\mathbf{x}}_r, \vec{\mathbf{x}}_{r'}, \omega))_{r,r'=1,\ldots,N}$ is applied to the recorded and time reversed signals before back propagation, then we obtain the IF imaging functional

$$\mathcal{I}^{\mathrm{IF}}(\vec{\mathbf{y}}^S) = \frac{1}{2\pi} \int d\omega \hat{\mathcal{I}}^{\mathrm{IF}}(\vec{\mathbf{y}}^S, \omega)\,, \tag{5}$$

where

$$\hat{\mathcal{I}}^{\mathrm{IF}}(\vec{\mathbf{y}}^S, \omega) = \sum_{r,r'=1}^{N} \hat{G}(\vec{\mathbf{y}}^S, \vec{\mathbf{x}}_r, \omega) \hat{K}(\vec{\mathbf{x}}_r, \vec{\mathbf{x}}_{r'}, \omega) \overline{\hat{P}(\vec{\mathbf{x}}_{r'}, \omega)}\,. \tag{6}$$

The purpose of this paper is to introduce and analyze a universal way to choose the filter $\hat{K}$ so that refocusing on the active sources is better than with the standard KM method, in which case $\hat{K}$ is the identity matrix.

2.2. Active imaging

In active imaging (Figure 1, right) the object that we want to image is a reflector or a distribution of reflectors. The array sensors at $\{\vec{\mathbf{x}}_s, s = 1, \ldots, N\}$ emit one at a time pulses $f(\vec{\mathbf{x}}_s, t)$ that illuminate the reflectors and the backscattered signals $P(\vec{\mathbf{x}}_r, \vec{\mathbf{x}}_s, t)$ are recorded by the array sensors at $\{\vec{\mathbf{x}}_r, r = 1, \ldots, N\}$. For simplicity we assume in this paper that the same array is used for illumination and recording. If we denote by $\Pi(\vec{\mathbf{x}}_r, \vec{\mathbf{x}}_s, t)$ the array response matrix (i.e. the matrix of recorded signals when $f(\vec{\mathbf{x}}_s, t) = \delta(t)$), then the recorded signals have the form

$$\hat{P}(\vec{\mathbf{x}}_r, \vec{\mathbf{x}}_s, \omega) = \hat{\Pi}(\vec{\mathbf{x}}_r, \vec{\mathbf{x}}_s, \omega) \hat{f}(\vec{\mathbf{x}}_s, \omega) \tag{7}$$

in the frequency domain. The KM imaging functional at the search point $\vec{\mathbf{y}}^S$ is of the form (1) with

$$\hat{\mathcal{I}}^{\mathrm{KM}}(\vec{\mathbf{y}}^S, \omega) = \sum_{r,s=1}^{N} \hat{G}(\vec{\mathbf{y}}^S, \vec{\mathbf{x}}_r, \omega) \overline{\hat{P}(\vec{\mathbf{x}}_r, \vec{\mathbf{x}}_s, \omega)} \hat{G}(\vec{\mathbf{x}}_s, \vec{\mathbf{y}}^S, \omega)\,. \tag{8}$$

Note that this KM functional is different from time reversal with data from active probing because we backpropagate from the source locations as well as from the receiver locations. Imaging with KM is closely related to linearized least squares [7, 8]. As in passive array imaging, if a filter $(\hat{K}(\vec{\mathbf{x}}_r, \vec{\mathbf{x}}_{r'}, \omega))_{r,r'=1,\dots,N}$ is applied before numerical back propagation of the recorded signals from both sources and receivers, then the imaging functional is of the form (5) with

$$\hat{\mathcal{I}}^{\mathrm{IF}}(\vec{\mathbf{y}}^S, \omega) = \sum_{r,r',s,s'=1}^{N} \hat{G}(\vec{\mathbf{y}}^S, \vec{\mathbf{x}}_r, \omega)\hat{K}(\vec{\mathbf{x}}_r, \vec{\mathbf{x}}_{r'}, \omega)\overline{\hat{P}(\vec{\mathbf{x}}_{r'}, \vec{\mathbf{x}}_{s'}, \omega)}\hat{K}(\vec{\mathbf{x}}_{s'}, \vec{\mathbf{x}}_s, \omega)\hat{G}(\vec{\mathbf{x}}_s, \vec{\mathbf{y}}^S, \omega)\,. \quad (9)$$

We will show that it is possible to choose the filter $\hat{K}$ so as to enhance refocusing on the reflectors. We could also try to optimize the illumination $\hat{f}(\vec{\mathbf{x}}_s, \omega)$, but this is a different problem that can be considered separately [7, 8]. Here we will assume that $\hat{f}(\vec{\mathbf{x}}_s, \omega)$ is fixed and known. The analysis is carried out for passive imaging, since the reflectors can be interpreted as secondary sources in the Born approximation. The analysis carries over to the active source case.

3. Least squares filter

3.1. Optimal refocusing for passive imaging

In order to study the least square problem that determines the expression of the inverse filter $\hat{K}$, we consider the passive imaging configuration in which a point source emits a pulse $f(t)$ of the form

$$f(t) = \frac{1}{2}e^{-i\omega_0 t} f_B(t) + c.c.\,, \quad (10)$$

where f_B is bandlimited with bandwidth B. If there is no electronic or other additive noise and there is a unique source in the medium, then the recorded signals are

$$\hat{P}(\vec{\mathbf{x}}_r, \omega) = \hat{G}(\vec{\mathbf{x}}_r, \vec{\mathbf{y}}, \omega)\hat{f}(\omega)\,, \quad (11)$$

where $\vec{\mathbf{y}}$ is the location of the source and the time-harmonic Green's function $\hat{G}$ is (3) in three dimensions and (4) in two dimensions.

The main goal is to choose the filter $\hat{K}$ so as to optimize refocusing at each frequency. To assess the quality of refocusing, we introduce a control array at $\{\vec{\mathbf{y}}_q, q = 1, \dots, N_q\}$. The source location belongs to this control array. We want to find a filter that optimally refocuses on this array. That is, if $\vec{\mathbf{y}}_{q_0}$ is the source location, then the imaging functional refocuses at $\vec{\mathbf{y}}_{q_0}$ while putting as little energy as possible on the other points of the array $\{\vec{\mathbf{y}}_q, q \neq q_0\}$. With the source at $\vec{\mathbf{y}}_{q_0}$, the L^2-error over the control array is

$$\mathcal{E}^2_{q_0}(\omega, \hat{K}) = \sum_{q=1}^{N_q} \left| \hat{\mathcal{I}}^{\mathrm{IF}}(\vec{\mathbf{y}}_q, \vec{\mathbf{y}}_{q_0}, \omega) - \overline{\hat{f}(\omega)\hat{S}(\vec{\mathbf{y}}_q, \vec{\mathbf{y}}_{q_0}, \omega)} \right|^2, \quad (12)$$

where

$$\hat{S}(\vec{\mathbf{y}}_q, \vec{\mathbf{y}}_{q_0}, \omega) = \mathbf{1}_{q_0}(q), \quad q = 1, \dots, N_q\,,$$

is the target N_q-dimensional vector, that is, a signal of amplitude one at the position $\vec{\mathbf{y}}_{q_0}$ and of amplitude zero at the other elements of the array $\{\vec{\mathbf{y}}_q, q \neq q_0\}$. The imaging functional is given by (6), which has the form

$$\hat{\mathcal{I}}^{\mathrm{IF}}(\vec{\mathbf{y}}_q, \vec{\mathbf{y}}_{q_0}, \omega) = (\mathcal{G}\hat{K}\mathcal{G}^\star)_{qq_0}\overline{\hat{f}(\omega)}\,. \tag{13}$$

Here

$$\mathcal{G}(\omega) = (\hat{G}(\vec{\mathbf{y}}_q, \vec{\mathbf{x}}_r, \omega))_{q=1,\ldots,N_q,\, r=1,\ldots,N} \tag{14}$$

is the $N_q \times N$-matrix of time-harmonic Green's functions from the sensor array to the control array and the star $\star$ denotes conjugate and transpose.

Since in imaging the source position is not known, the optimization criterion is taken as the minimization of the L^2-error for refocusing over all possible source positions on the control array:

$$\mathcal{E}^2(\omega, \hat{K}) = \sum_{q_0=1}^{N_q} \mathcal{E}^2_{q_0}(\omega, \hat{K})\,.$$

This can be expressed as

$$\mathcal{E}^2(\omega, \hat{K}) = \mathrm{Tr}\left(\mathcal{G}\hat{K}^\star\mathcal{G}^\star\mathcal{G}\hat{K}\mathcal{G}^\star - \mathcal{G}\hat{K}^\star\mathcal{G}^\star - \mathcal{G}\hat{K}\mathcal{G}^\star + I_{N_q}\right)|\hat{f}(\omega)|^2\,,$$

where I_{N_q} is the $N_q \times N_q$-identity matrix.

We now introduce the nonnegative Hermitian $N \times N$-matrix

$$\mathcal{Q}(\omega) = \mathcal{G}^\star(\omega)\mathcal{G}(\omega)\,. \tag{15}$$

This is the time-reversal matrix when the array $\{\vec{\mathbf{x}}_r, r = 1, \ldots, N\}$ carries the sources and the array $\{\vec{\mathbf{y}}_q, q = 1, \ldots, N_q\}$ is the time-reversal array. With this notation, the global error has the form

$$\mathcal{E}^2(\omega, \hat{K}) = \left[\mathrm{Tr}\left(\hat{K}^\star\mathcal{Q}\hat{K}\mathcal{Q} - \hat{K}^\star\mathcal{Q} - \hat{K}\mathcal{Q}\right) + N_q\right]|\hat{f}(\omega)|^2\,.$$

This is a quadratic functional in $\hat{K}$ that depends only on $\mathcal{Q}$. Therefore the solution of the minimization problem depends only on $\mathcal{Q}$. We see that $\hat{K}$ is a minimizer if it satisfies the condition

$$\mathcal{Q}\hat{K}\mathcal{Q} = \mathcal{Q}\,. \tag{16}$$

If $\mathcal{Q}(\omega)$ is invertible then the unique solution of the minimization problem is the $N \times N$-matrix

$$\hat{K}_{\mathrm{LS}}(\omega) = \mathcal{Q}(\omega)^{-1} = (\mathcal{G}(\omega)^\star\mathcal{G}(\omega))^{-1}\,, \tag{17}$$

and the minimum error is

$$\mathcal{E}^2(\omega, \hat{K}_{\mathrm{LS}}) = |\hat{f}(\omega)|^2\,[N_q - N]\,. \tag{18}$$

For the matrix $\mathcal{Q}$ to be invertible it is necessary that the number of rows of the matrix $\mathcal{G}$ in (15) be larger than the number of columns, i.e. $N_q \geq N$. This result shows that if $\mathcal{Q}$ is invertible and $N = N_q$, then perfect refocusing can be achieved. In the general

case $N_q > N$, it is remarkable that the error depends only on $N_q - N$. This indicates that it is theoretically possible to construct an efficient inverse filter when the sensor array is dense, even if its size is small.

If $\mathcal{Q}(\omega)$ is not invertible, then the solution for the minimization problem is not unique. This degeneracy occurs when there exists a non-zero N-dimensional vector v such that $\mathcal{G}^\star\mathcal{G}v = 0$, which means that if the array $\{\vec{\mathbf{x}}_r, r = 1, \dots, N\}$ emits the signal $v = (v_r)_{r=1,\dots,N}$, and the array $\{\vec{\mathbf{y}}_q, q = 1, \dots, N_q\}$ records, time-reverses and re-emits the signals, then no refocusing occurs at the array $\{\vec{\mathbf{x}}_r, r = 1, \dots, N\}$. In this degenerate case one solution is the pseudo-inverse of $\mathcal{Q}$, but there are many solutions. Let us introduce the singular value decomposition of the matrix $\mathcal{G}$:

$$\mathcal{G}(\omega) = \mathcal{U}(\omega)\Sigma(\omega)\mathcal{V}(\omega)^\star\,, \tag{19}$$

where $\mathcal{U}$ is a $N_q \times N_q$ unitary matrix, $\mathcal{V}$ is a $N \times N$ unitary matrix, Σ is a $N_q \times N$ matrix with nonincreasing nonnegative numbers on the diagonal and zeros off the diagonal. We have $\mathcal{G}\mathcal{V} = \mathcal{U}\Sigma$ and $\mathcal{G}^\star\mathcal{U} = \mathcal{V}\Sigma$. The matrix $\mathcal{Q}$ can then be written as $\mathcal{Q} = \mathcal{V}\Sigma^\star\Sigma\mathcal{V}^\star$. If we denote by p the rank of $\mathcal{Q}$, then $\Sigma^\star\Sigma$ is a $N \times N$ diagonal matrix with diagonal coefficients $(\sigma_1^2, \dots, \sigma_p^2, 0, \dots, 0)$, where the σ_j are positive. With this formulation, the solutions $\hat{K}$ are the $N \times N$-matrices of the form

$$\hat{K}_{\mathrm{LS},\alpha}(\omega) = \mathcal{V}(\omega)\mathrm{diag}(\sigma_1^{-2}(\omega), \dots, \sigma_p^{-2}(\omega), \alpha_{p+1}(\omega), \dots, \alpha_N(\omega))\mathcal{V}(\omega)^\star\,,$$

where the real vector $\alpha(\omega) = (\alpha_j(\omega))_{j=p+1,\dots,N}$ can be chosen arbitrarily. The particular choice $\alpha = 0$ corresponds to the pseudo-inverse. For any choice of α we have

$$\hat{\mathcal{I}}^{\mathrm{IF}}(\vec{\mathbf{y}}_q, \vec{\mathbf{y}}_{q_0}, \omega) = (\mathcal{U}(\omega)\mathrm{diag}(1, \dots, 1, 0, \dots, 0)\mathcal{U}(\omega)^\star)_{qq_0}\,,$$

where the $N_q \times N_q$ diagonal matrix has p coefficients equal to one, and the minimum error is then

$$\mathcal{E}^2(\omega, \hat{K}_{\mathrm{LS},\alpha}) = |\hat{f}(\omega)|^2\,[N_q - p]\ . \tag{20}$$

3.2. Least squares filter in the presence of noise

We consider again the least squares analysis in the presence of additive noise in the recorded signals and show that the LS filter is stable with respect to this noise.

Let us assume that the recorded signals have the form

$$\hat{P}(\vec{\mathbf{x}}_r, \omega) = \hat{G}(\vec{\mathbf{x}}_r, \vec{\mathbf{y}}_{q_0}, \omega)\hat{f}(\omega) + \hat{\epsilon}_r(\omega)\,, \tag{21}$$

where $\vec{\mathbf{y}}_{q_0}$ is the source position and $\hat{\epsilon}_r(\omega)$, $r = 1, \dots, N$ is a zero-mean complex Gaussian vector with covariance

$$\mathbb{E}[\hat{\epsilon}_r(\omega)\overline{\hat{\epsilon}}_{r'}(\omega)] = \sigma_\omega^2\mathbf{1}_r(r')\,.$$

The mean squared global error is then

$$\mathbb{E}[\mathcal{E}^2(\omega, \hat{K})] = \left[\mathrm{Tr}\left(\hat{K}^\star\mathcal{Q}\hat{K}\mathcal{Q} - \hat{K}^\star\mathcal{Q} - \hat{K}\mathcal{Q} + \sigma_\omega^2 N_q\hat{K}^\star\mathcal{Q}\hat{K}\right) + N_q\right]|\hat{f}(\omega)|^2\,.$$

This is also a quadratic functional that depends only on $\mathcal{Q}$ and σ_ω^2. It follows that $\hat{K}$ is a minimizer if it solves the equation

$$\mathcal{Q}\hat{K}\mathcal{Q} + N_q\sigma_\omega^2\mathcal{Q}\hat{K} = \mathcal{Q}\,.$$

Since $\mathcal{Q}$ is nonnegative, the matrix $\mathcal{Q} + N_q\sigma_\omega^2 I_N$ is invertible and the condition can also be written as

$$\mathcal{Q}\hat{K} = \mathcal{Q}(\mathcal{Q} + N_q\sigma_\omega^2 I_N)^{-1}\,. \tag{22}$$

If $\mathcal{Q}(\omega)$ is invertible, then the unique solution of the minimization problem is the $N \times N$-matrix

$$\hat{K}_{\mathrm{LS}}(\omega) = (\mathcal{Q} + N_q\sigma_\omega^2 I_N)^{-1}\,, \tag{23}$$

and the minimum error is

$$\mathbb{E}[\mathcal{E}^2(\omega, \hat{K}_{\mathrm{LS}})] = |\hat{f}(\omega)|^2\left[N_q - \sum_{j=1}^{N}\frac{\sigma_j^2(\omega)}{\sigma_j^2(\omega) + N_q\sigma_\omega^2}\right], \tag{24}$$

where the $\sigma_j(\omega)$, $j = 1, \ldots, N$, are the singular values of $\mathcal{G}(\omega)$.

If $\mathcal{Q}(\omega)$ is not invertible, then using the SVD we see that there is a family of solutions for the minimization problem that have the form

$$\hat{K}_{\mathrm{LS},\alpha}(\omega) = \mathcal{V}(\omega)\mathrm{diag}\Big(\frac{1}{\sigma_1^2(\omega) + N_q\sigma_\omega^2}, \ldots, \frac{1}{\sigma_p^2(\omega) + N_q\sigma_\omega^2}, \alpha_{p+1}(\omega), \ldots, \alpha_N(\omega)\Big)\mathcal{V}(\omega)^\star\,, \tag{25}$$

where the real vector $(\alpha_j(\omega))_{j=p+1,\ldots,N}$ can be chosen arbitrarily. The minimal error is still given by (24). Note that (23) is the element of this family for which $\alpha_j(\omega) = 1/(N_q\sigma_\omega^2)$.

3.3. Comments on the use of the inverse filter

Refocusing can be significantly improved by using the IF, compared to KM. However, there are two issues to be considered. First, the matrix $\mathcal{Q}(\omega) = \mathcal{G}^\star(\omega)\mathcal{G}(\omega)$, even if it is invertible, can be severely ill-conditioned and its inversion then requires numerical regularization. Second, this matrix depends on the control array, since it is given in terms of the matrix $\mathcal{G}(\omega)$ of time-harmonic Green's functions from the sensor array to the control array. We show in the next section that it is possible to find a universal form for the LS filter for a large class of control arrays, and that the trade-off between resolution enhancement and numerical regularization can be studied in detail. The extension of the analysis above to active imaging is carried out in Appendix B.

4. The universal kernel

The LS filter (17) depends on the medium and on the choice of the control array in which the source or reflector is embedded. However, it is possible to find an analytic expression for the filter when the source or reflector is in the far field, that is, when its distance from the sensor array is much larger than the wavelength, and when the

control array forms a closed surface around the sensor array. With this choice of control array the LS filter $\hat{K}_{\rm LS}$ is proportional to the inverse of the sinc matrix

$$\Big(SI(\vec{\mathbf{x}}_r,\vec{\mathbf{x}}_{r'},\omega)\Big)_{r,r'=1,\ldots,N}=\Big(\mathrm{sinc}\Big(\frac{\omega}{c_0}|\vec{\mathbf{x}}_r-\vec{\mathbf{x}}_{r'}|\Big)\Big)_{r,r'=1,\ldots,N}\,, \tag{26}$$

which depends only on the location of the sensors on the array. This is valid in a three-dimensional medium that is smoothly varying around the sensor array and is homogeneous near the control array and in its exterior (see Appendix A). In a two-dimensional medium, the LS filter $\hat{K}_{\rm LS}$ is (proportional to) the inverse matrix of

$$\Big(SI(\vec{\mathbf{x}}_r,\vec{\mathbf{x}}_{r'},\omega)\Big)_{r,r'=1,\ldots,N}=\left(\frac{c_0}{\omega}J_0\Big(\frac{\omega}{c_0}|\vec{\mathbf{x}}_r-\vec{\mathbf{x}}_{r'}|\Big)\right)_{r,r'=1,\ldots,N}\,. \tag{27}$$

The following are some basic properties of the sinc matrix (26) and its inverse:

1) The matrix SI is nonnegative, real, and symmetric. Its eigenvalues are $\mu^1\geq\cdots\geq\mu^N\geq 0$, with the corresponding orthonormal real-valued eigenvectors $(\psi_r^n(\omega))=\psi^n,\ n=1,\ldots,N$:

$$\sum_{r'=1}^{N}SI(\vec{\mathbf{x}}_r,\vec{\mathbf{x}}_{r'},\omega)\psi_{r'}^n(\omega)=\mu^n(\omega)\psi_r^n(\omega)\,,\quad r=1,\ldots,N\,. \tag{28}$$

For linear and regularly arranged sensor array the (r,r')-entry of the matrix SI depends only on $|r'-r|$, which means that the matrix SI is Toeplitz. The eigenfunctions are then the discrete prolate spheroidal sequences, which have been studied in detail in [20].

2) If the distance between sensors on the array is a multiple of $\lambda/2$, then the sinc matrix is the identity. This is also approximately true when the array sensors are far from each other, relative to the wavelength. This indicates that KM is the optimal filter if the array is not oversampled, as noted in [27].

3) If the array is undersampled, which means that distances between sensors are larger than $\lambda/2$, then the sinc matrix is well-conditioned and can be inverted easily.

4) If the array is oversampled, which means that distances between sensors are smaller than $\lambda/2$, then the sinc matrix is ill-conditioned and has very small eigenvalues (see Appendix D). This is the case where resolution can be improved by using the inverse filter. The inversion is done with numerical filtering [26, 28], which amounts to neglecting the smallest eigenvalues. Motivated by the analysis of Subsection 3.2 we consider the following regularized inverse

$$\hat{K}_{\rm LS}(\vec{\mathbf{x}}_r,\vec{\mathbf{x}}_{r'},\omega)=\sum_{n=1}^{N}\frac{1}{\mu_c^\omega+\mu^n(\omega)}\psi_r^n(\omega)\psi_{r'}^n(\omega)\,. \tag{29}$$

By comparing with Eqs. (23)-(25), we see that this inverse filter is optimal when there is additive noise of the form (21), for a suitable choice of μ_c^ω.

The choice of the regularization number $\mu_c^\omega\geq 0$, which can depend on ω, should reflect the trade-off between resolution enhancement and SNR degradation. This is an important issue that will be discussed in detail in the next sections. The basic idea is that if we take $\mu_c^\omega=0$ or close to 0, then use of the inverse sinc matrix enhances very significantly refocusing, but noise is also amplified. If we take μ_c^ω too large, then the

inversion is easy and noise is not amplified, but resolution is not enhanced. In fact, for μ_c^ω very large, the inverse kernel becomes proportional to $\sum_n \psi_r^n(\omega)\psi_{r'}^n(\omega) = \mathbf{1}_r(r')$ and the inverse filter is then simply the identity. Other regularization methods could be chosen, such as the Tikhonov regularization method [25] where the term $1/[\mu_c^\omega + \mu^n]$ in (29) is replaced by $\mu^n/[(\mu_c^\omega)^2 + (\mu^n)^2]$, or the truncation method where the term $1/[\mu_c^\omega + \mu^n]$ in (29) is replaced by $[1/\mu^n]\mathbf{1}_{\mu^n \geq \mu_c^\omega}$, or the generalized cross-validation method [15, 12], which is a Tikhonov-type method where the regularization parameter $(\mu_c^\omega)^2$ is chosen adaptively. A review of regularisation methods can be found in [3, 1]. These methods can be used instead of numerical filtering (29), but we have not seen any improvement or advantage in our numerical simulations. The theoretical analysis of Subsection 3.2 shows that the optimal filter in the presence of additive noise is indeed of the form (29).

In two dimensions the matrix SI has the same properties as those of SI in three dimensions except for a few differences related to oversampling and undersampling:
1) The zeros of the Bessel function J_0 are not regularly spaced, so the matrix SI is not equal or proportional to the identity for any spacing of the sensors of the array.
2) The power-law decay of the function $J_0(x)$ is $x^{-1/2}$, instead of x^{-1} for $\mathrm{sinc}(x)$. Therefore the off-diagonal terms are more important in 2D than in 3D, and the inverse filter plays a more important role in the undersampled situation.
3) The factor $1/\omega$ in the expression (27) of the matrix SI is important in broadband imaging. It means that in the case of well separated sensors, the inverse filter is proportional to the identity matrix times ω. This implies that the time-derivative of the KM functional imaging has a better resolution than the KM functional imaging itself.

5. Numerical simulations

Before going into the detailed resolution and SNR analysis of the IF imaging method, we present the results of a few numerical simulations that illustrate the enhancement of cross range resolution. In the numerical simulations we take 9 sensors on a linear array at a distance $\lambda_0/8$ from each other, along the x-axis. Here $\lambda_0 = 2\pi c_0/\omega_0$ is the carrier wavelength and the length of the array is λ_0. We use frequency-dependent regularization numbers of the form $\mu_c^\omega = \mu_c\omega_0/\omega$, where μ_c is a frequency-independent parameter to be chosen empirically or by an adaptive algorithm, as described in Subsection 8.3. In units of central wavelengths, so that $\lambda_0 = 1$, and with time units such that $c_0 = 1$, the bandwidth B is one percent of the carrier frequency $\omega_0 = 2\pi$, and the sampling frequency is ten times smaller than the bandwidth. This means that the recording time window for the data is ten times the pulse duration $2\pi/B = 100$.

In Figures 2-5 we plot the images obtained for two point sources. They show clearly the enhancement of cross range resolution and the loss of stability of the IF method compared to the standard KM method.

In Figures 6-7 we plot the results obtained with an active array and two small reflectors at the same range (which is a difficult case). In Figure 6 (with no noise) we show that it is possible to image the two reflectors with much better resolution using

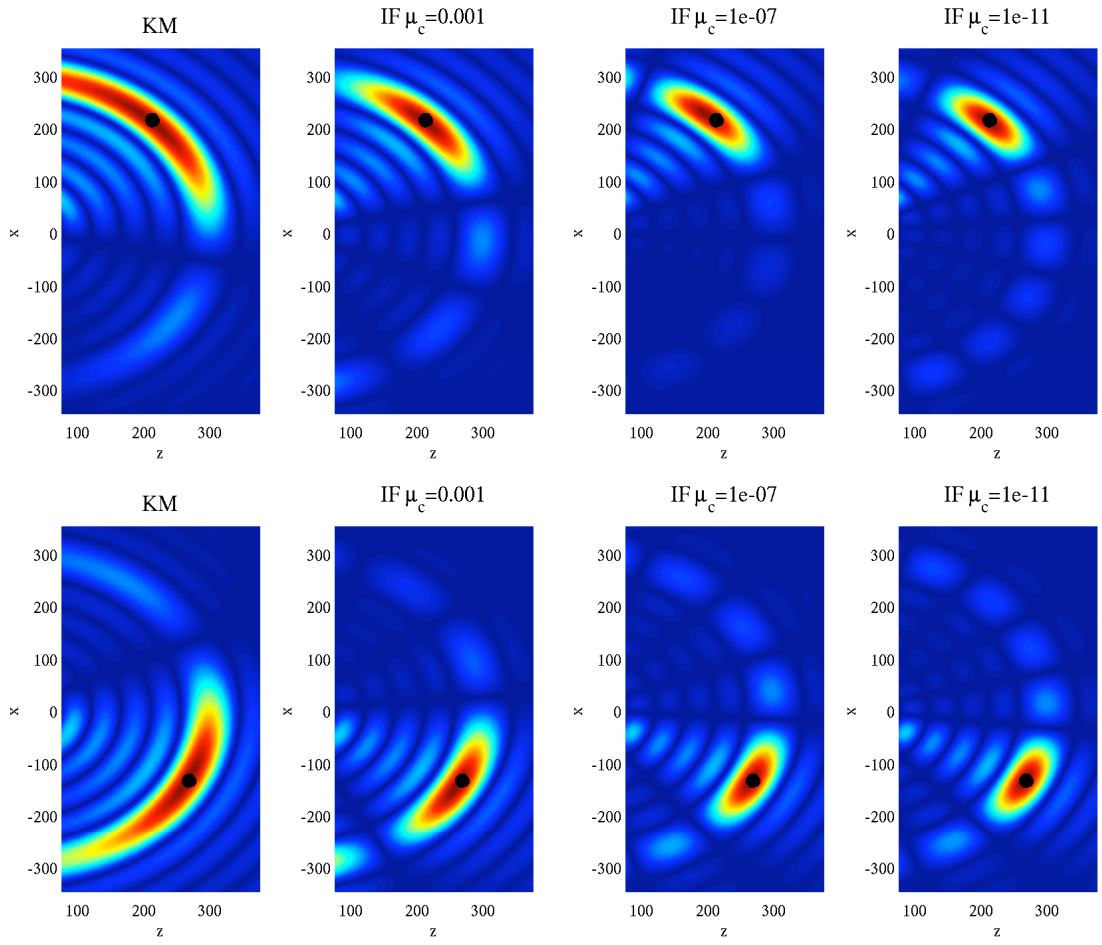

Figure 2. Passive imaging of a source located at $(x, z) = 300(\sin\theta, \cos\theta)$, with $\theta = 0.25\pi$ (top) and $\theta = -0.15\pi$ (bottom). The linear array is centered at $(0, 0)$ and has 9 sensors that are $1/8$ apart, with distances measure in units of the central wavelength. There is no noise (infinite SNR), which allows us to take an arbitrarily small value of the regularization number μ_c and to get dramatic cross range resolution enhancement compared to KM.

the IF filter than with KM. However, the inverse filter is applied twice and so noise is also more amplified. Therefore, more regularization is necessary in a noisy case in order to get a stable image (Figure 7).

6. Resolution analysis in the continuum case

In this section we consider passive imaging in a three-dimensional homogeneous medium and assume that the sensors are placed along the segment $\vec{\mathbf{x}} \in [-a/2, a/2] \times \{0\} \times \{0\}$, separated by $h \ll \lambda_0$. We also assume that there is a source at $\vec{\mathbf{y}}$ emitting the pulse (10) and that there is no noise, so that the recorded signals are given by (11). With this configuration we can use the prolate spheroidal functions and get explicit expressions for the imaging functionals.

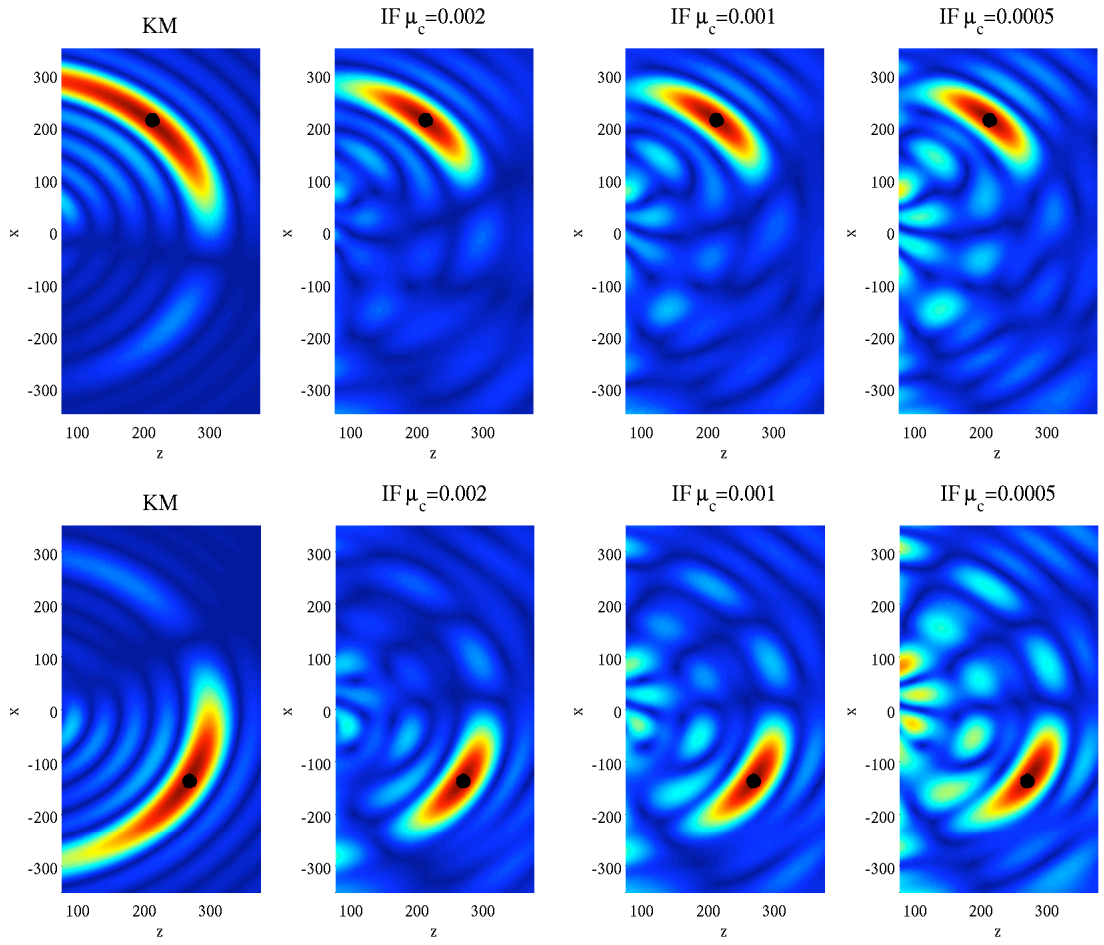

Figure 3. Passive imaging of a source located at $(x, z) = 300(\sin\theta, \cos\theta)$, with $\theta = 0.25\pi$ (top) and $\theta = -0.15\pi$ (bottom). The array configuration is as in the previous figure. Here the noise level of the data is SNR=10 dB. We choose $\mu_c \simeq 10^{-3}$ to get a stable image, which gives significant cross range resolution enhancement. The standard KM method is not affected by such a noise level.

6.1. The KM imaging functional

In the continuum limit the KM imaging functional at the search point $\vec{\mathbf{y}}^S$ is

$$\hat{\mathcal{I}}^{\mathrm{KM}}(\vec{\mathbf{y}}^S, \omega) = \frac{1}{h}\int_{-\frac{a}{2}}^{\frac{a}{2}} \hat{G}(\vec{\mathbf{y}}^S, (x_r, 0, 0), \omega)\overline{\hat{G}((x_r, 0, 0), \vec{\mathbf{y}}, \omega)}dx_r\overline{\hat{f}(\omega)}\,. \qquad (30)$$

In this section we assume that the range, i.e. the distance $|\vec{\mathbf{y}}|$ from the source to the center of the array, is much larger than the diameter of the array a, and that $(\omega_0/c_0)a^2 \ll |\vec{\mathbf{y}}|$. This is the Fraunhofer diffraction regime, which allows us to use the following approximation of the Green's function from a point $\vec{\mathbf{x}}_r$ of the sensor array to a point $\vec{\mathbf{y}}^S$ in the vicinity of the source:

$$\hat{G}(\vec{\mathbf{x}}_r, \vec{\mathbf{y}}^S, \omega) \simeq \frac{e^{i\frac{\omega}{c_0}|\vec{\mathbf{y}}^S|}}{4\pi|\vec{\mathbf{y}}^S|}e^{-i\frac{\omega}{c_0}\frac{\vec{\mathbf{x}}_r\cdot\vec{\mathbf{y}}^S}{|\vec{\mathbf{y}}^S|}}\,. \qquad (31)$$

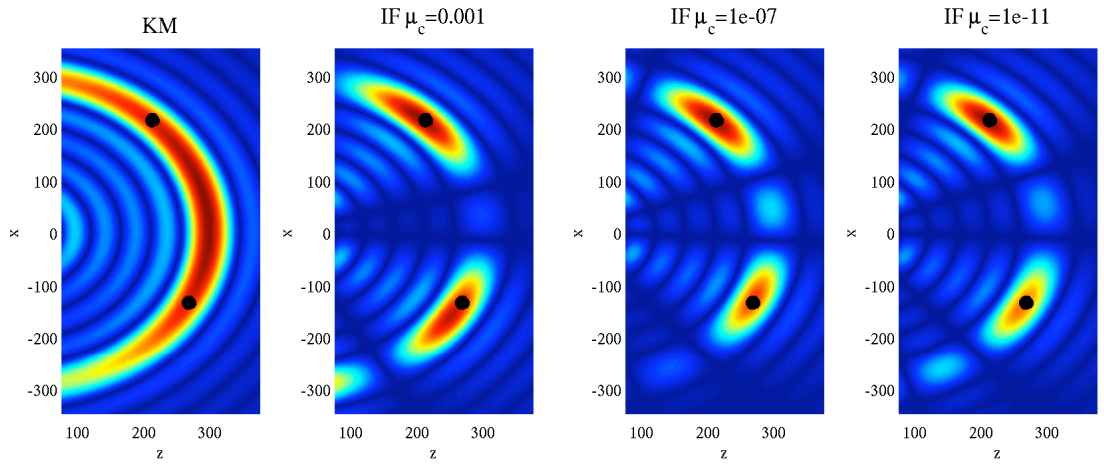

Figure 4. Passive imaging of two sources located at $300(\sin\theta_1, \cos\theta_1)$ and $300(\sin\theta_2, \cos\theta_2)$, with $\theta_1 = 0.25\pi$ and $\theta_2 = -0.15\pi$. The array configuration is the same as in the previous figures. Here there is no noise (infinite SNR).

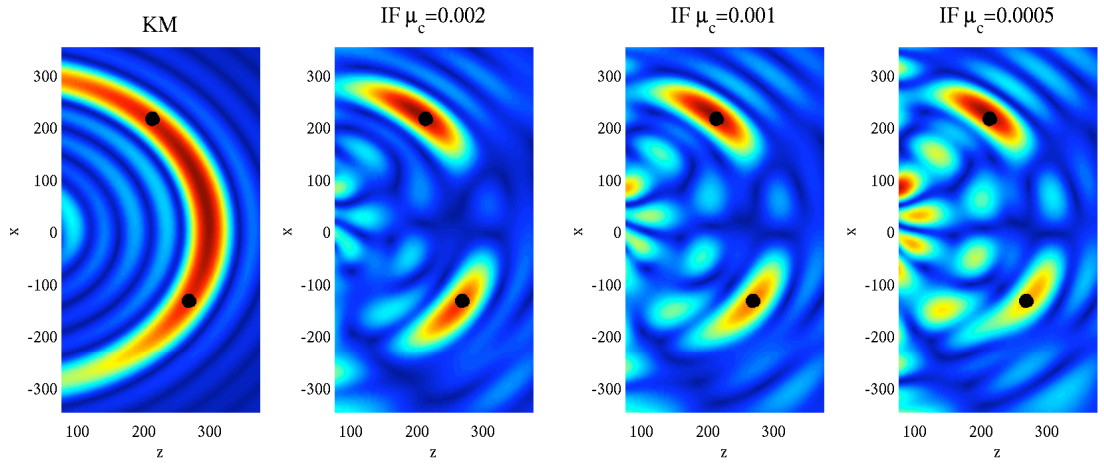

Figure 5. Passive imaging of two point sources located at $300(\sin\theta_1, \cos\theta_1)$ and $300(\sin\theta_2, \cos\theta_2)$, with $\theta_1 = 0.25\pi$ and $\theta_2 = -0.15\pi$. The array configuration is the same as in the previous figures. Here the noise level is SNR=10 dB.

This approximation comes from a direct expansion of the distance $|\vec{\mathbf{x}}_r - \vec{\mathbf{y}}^S|$ in the expression of the full Green's function (3) which, as already noted, is valid when $|\vec{\mathbf{x}}_r| \ll |\vec{\mathbf{y}}^S|$ and $(\omega/c_0)|\vec{\mathbf{x}}_r|^2 \ll |\vec{\mathbf{y}}^S|$.

As a result, for any search point $\vec{\mathbf{y}}^S$ such that $\left||\vec{\mathbf{y}}| - |\vec{\mathbf{y}}^S|\right| \ll |\vec{\mathbf{y}}|$ we have

$$\hat{\mathcal{I}}^{\mathrm{KM}}(\vec{\mathbf{y}}^S, \omega) = \frac{a}{16\pi^2|\vec{\mathbf{y}}|^2 h}\mathrm{sinc}\left[\frac{\omega a}{2c_0|\vec{\mathbf{y}}|}(\xi^S - \xi)\right] e^{i\frac{\omega}{c_0}(|\vec{\mathbf{y}}^S| - |\vec{\mathbf{y}}|)}\overline{\hat{f}(\omega)}\,, \tag{32}$$

where ξ^S and ξ are the first coordinates of the search and source points $\vec{\mathbf{y}}^S$ and $\vec{\mathbf{y}}$.

In the time domain, we have

$$\mathcal{I}^{\mathrm{KM}}(\vec{\mathbf{y}}^S) = \frac{a}{32\pi^3|\vec{\mathbf{y}}|^2 h}\int \mathrm{sinc}\left[\frac{\omega a}{2c_0|\vec{\mathbf{y}}|}(\xi^S - \xi)\right] e^{i\frac{\omega}{c_0}(|\vec{\mathbf{y}}^S| - |\vec{\mathbf{y}}|)}\overline{\hat{f}(\omega)}d\omega\,. \tag{33}$$

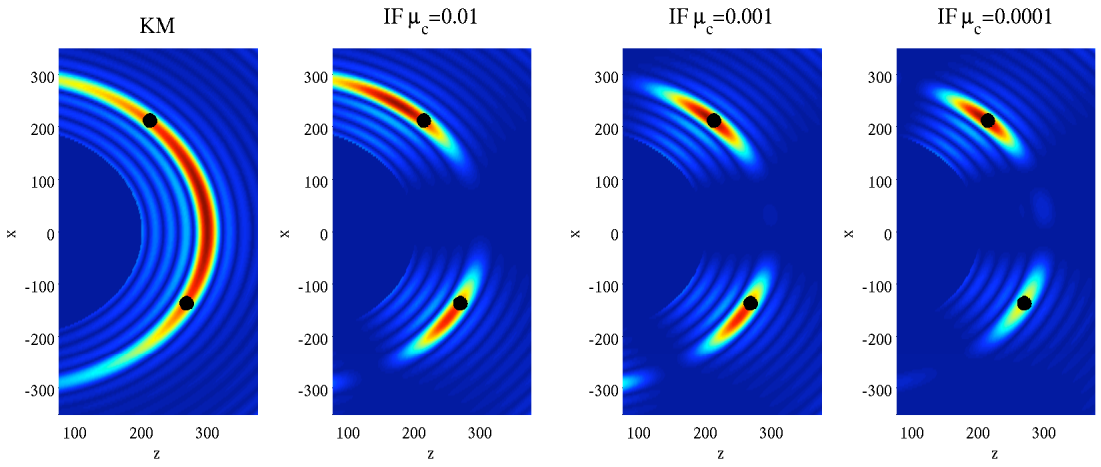

Figure 6. Active imaging of two point reflectors located at $300(\sin\theta_1, \cos\theta_1)$ and $300(\sin\theta_2, \cos\theta_2)$, with $\theta_1 = 0.25\pi$ and $\theta_2 = -0.15\pi$. The array configuration is the same as in the previous figures. Here there is no noise (infinite SNR).

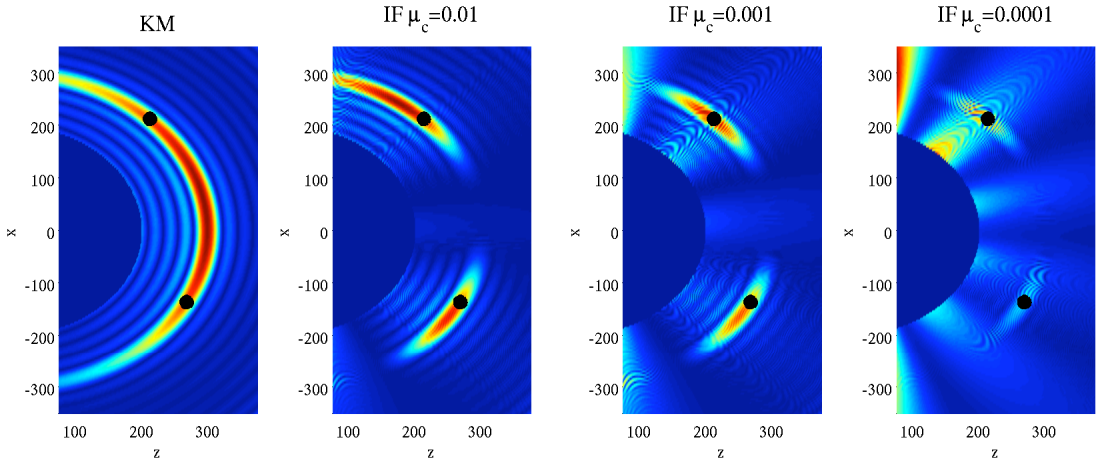

Figure 7. Active imaging of two point reflectors located at $300(\sin\theta_1, \cos\theta_1)$ and $300(\sin\theta_2, \cos\theta_2)$, with $\theta_1 = 0.25\pi$ and $\theta_2 = -0.15\pi$. The array configuration is the same as in previous figures. Here the noise level is SNR=20 dB.

If we assume that the pulse is a sinc with carrier frequency ω_0 and bandwidth $B \ll \omega_0$ so that

$$\hat{f}_B(\omega) = \frac{2\pi}{B}\mathbf{1}_{(-B/2,B/2)}(\omega), \quad f_B(t) = \mathrm{sinc}\Big(\frac{Bt}{2}\Big), \quad f(t) = \cos(\omega_0 t)\mathrm{sinc}\Big(\frac{Bt}{2}\Big), \quad (34)$$

then

$$\mathcal{I}^{\mathrm{KM}}(\vec{\mathbf{y}}^S) = \frac{a}{16\pi^2|\vec{\mathbf{y}}|^2 h}\mathrm{sinc}\left(\frac{B(|\vec{\mathbf{y}}^S| - |\vec{\mathbf{y}}|)}{2c_0}\right)\cos\left(\frac{\omega_0(|\vec{\mathbf{y}}^S| - |\vec{\mathbf{y}}|)}{c_0}\right)$$
$$\times\ \mathrm{sinc}\Big[\frac{\omega_0 a}{2c_0|\vec{\mathbf{y}}|}(\xi^S - \xi)\Big]. \quad (35)$$

This shows that the cross range resolution is controlled by the carrier frequency ω_0 and is given by $|\vec{\mathbf{y}}|\lambda_0/a$, while the range resolution is controlled by the bandwidth B and is given by $2\pi c_0/B$.

6.2. The IF imaging functional

The imaging functional when using the inverse filter is proportional to

$$\hat{\mathcal{I}}^{\rm IF}(\vec{\mathbf{y}}^S,\omega)=\frac{\overline{\hat{f}(\omega)}}{h^2}\int_{-\frac{a}{2}}^{\frac{a}{2}}\int_{-\frac{a}{2}}^{\frac{a}{2}}\hat{G}(\vec{\mathbf{y}}^S,(x_r,0,0),\omega)\hat{K}_{\rm LS}(x_r,x_{r'},\omega)\overline{\hat{G}((x_{r'},0,0),\vec{\mathbf{y}},\omega)}dx_r dx_{r'}\,.$$

The inverse kernel $\hat{K}_{\rm LS}$ can be constructed in terms of the prolate spheroidal functions $\phi^n(x,C)$, which are the eigenfunctions of the sinc kernel [21]:

$$\int_{-1}^{1}\frac{\sin[C(x-y)]}{\pi(x-y)}\phi^n(y,C)dy=\eta^n(C)\phi^n(x,C)\,. \tag{36}$$

In Appendix C we give a brief review of the main properties of the prolate spheroidal functions. The eigenvalue problem for the inverse filter is

$$\frac{1}{h}\int_{-\frac{a}{2}}^{\frac{a}{2}}{\rm sinc}\Big[\frac{\omega}{c_0}(x-y)\Big]\psi^n(y,\omega)dy=\mu^n(\omega)\psi^n(x,\omega)\,,$$

and therefore the two eigenvalue-eigenvector families are related by

$$\mu^n(\omega)=\frac{\pi c_0}{\omega h}\eta^n\Big(\frac{\omega a}{2c_0}\Big),\quad \psi^n(y,\omega)=\sqrt{\frac{2h}{a}}\phi^n\Big(\frac{2y}{a},\frac{\omega a}{2c_0}\Big)\,. \tag{37}$$

Note that, by (C.2) and (C.3), ψ^n is normalized so that

$$\frac{1}{h}\int_{-\infty}^{\infty}\psi^n(y,\omega)\psi^m(y,\omega)dy=\mathbf{1}_m(n)\,,\qquad \frac{1}{h}\int_{-\frac{a}{2}}^{\frac{a}{2}}\psi^n(y,\omega)\psi^m(y,\omega)dy=\mathbf{1}_m(n)\eta^n\Big(\frac{\omega a}{2c_0}\Big)\,.$$

The standard KM method consists in taking instead of $\hat{K}_{\rm LS}$ the identity whose kernel is

$$\hat{K}^{\rm KM}(x,x',\omega)=h\,\delta(x-x')=\sum_{n=1}^{\infty}\frac{1}{\eta^n(\frac{\omega a}{2c_0})}\psi^n(x,\omega)\psi^n(x',\omega)\,. \tag{38}$$

The sinc kernel can be written as

$${\rm sinc}\Big[\frac{\omega}{c_0}(x-x')\Big]=\frac{\pi c_0}{\omega h}\sum_{n=1}^{\infty}\psi^n(x,\omega)\psi^n(x',\omega)\,. \tag{39}$$

The regularized inverse kernel is

$$\hat{K}_{\rm LS}(x,x',\omega)=\frac{\omega h}{\pi c_0}\sum_{n=1}^{\infty}\frac{1}{(\eta_c+\eta^n(\frac{\omega a}{2c_0}))\eta^n(\frac{\omega a}{2c_0})}\psi^n(x,\omega)\psi^n(x',\omega)\,. \tag{40}$$

If $\eta_c=0$ in this formula then we get the exact inverse. But as discussed in Section 4 we have introduced the regularization number η_c in order to ensure stability with respect to noise. We address this issue in the next section.

Using the inverse kernel (40), the imaging functional is given by

$$\hat{\mathcal{I}}^{\rm IF}(\vec{\mathbf{y}}^S,\omega)=\frac{\omega h}{16\pi^3 c_0|\vec{\mathbf{y}}^S||\vec{\mathbf{y}}|}\sum_{n=1}^{\infty}\frac{1}{(\eta_c+\eta^n(\frac{\omega a}{2c_0}))\eta^n(\frac{\omega a}{2c_0})}\hat{c}_n(\vec{\mathbf{y}}^S,\omega)\overline{\hat{c}_n(\vec{\mathbf{y}},\omega)}\overline{\hat{f}(\omega)}\,, \quad (41)$$

where

$$\hat{c}_n(\vec{\mathbf{y}},\omega)=\frac{4\pi|\vec{\mathbf{y}}|}{h}\int_{-\frac{a}{2}}^{\frac{a}{2}}\psi^n(x_r,\omega)\hat{G}((x_r,0,0),\vec{\mathbf{y}},\omega)dx_r\,. \quad (42)$$

Using the approximation (31) for the source point $\vec{\mathbf{y}}$, we have

$$\begin{aligned}\hat{c}_n(\vec{\mathbf{y}},\omega)&\simeq\frac{1}{h}e^{i\frac{\omega}{c_0}|\vec{\mathbf{y}}|}\int_{-\frac{a}{2}}^{\frac{a}{2}}\psi^n(x_r,\omega)e^{-i\frac{\omega}{c_0}x_r\frac{\xi}{|\vec{\mathbf{y}}|}}dx_r\\&=\sqrt{\frac{a}{2h}}e^{i\frac{\omega}{c_0}|\vec{\mathbf{y}}|}\int_{-1}^{1}\phi^n\Big(y_r,\frac{\omega a}{2c_0}\Big)e^{-i\frac{\omega a y_r}{2c_0}\frac{\xi}{|\vec{\mathbf{y}}|}}dy_r\\&=\sqrt{\frac{2\pi c_0}{\omega h}}\eta^n\Big(\frac{\omega a}{2c_0}\Big)^{1/2}i^{n+1}e^{i\frac{\omega}{c_0}|\vec{\mathbf{y}}|}\phi^n\Big(\frac{\xi}{|\vec{\mathbf{y}}|},\frac{\omega a}{2c_0}\Big)\,, \quad (43)\end{aligned}$$

where we have used the important property (C.7). Using the approximation (31) for the search point $\vec{\mathbf{y}}^S$ as well, we obtain

$$\hat{\mathcal{I}}^{\rm IF}(\vec{\mathbf{y}}^S,\omega)=\frac{1}{8\pi^2|\vec{\mathbf{y}}^S||\vec{\mathbf{y}}|}e^{i\frac{\omega}{c_0}(|\vec{\mathbf{y}}^S|-|\vec{\mathbf{y}}|)}\sum_{n=1}^{\infty}\frac{1}{\eta_c+\eta^n(\frac{\omega a}{2c_0})}\phi^n\Big(\frac{\xi^S}{|\vec{\mathbf{y}}^S|},\frac{\omega a}{2c_0}\Big)\phi^n\Big(\frac{\xi}{|\vec{\mathbf{y}}|},\frac{\omega a}{2c_0}\Big)\overline{\hat{f}(\omega)}\,.$$

If we assume that the pulse is a sinc with carrier frequency ω_0 and bandwidth $B\ll\omega_0$, so that the eigenvalues and eigenvectors do not vary too much with the parameter $\omega a/(2c_0)$ for ω in the bandwidth, then we obtain

$$\mathcal{I}^{\rm IF}(\vec{\mathbf{y}}^S)=\frac{1}{8\pi^2|\vec{\mathbf{y}}||\vec{\mathbf{y}}^S|}\mathrm{sinc}\left(\frac{B(|\vec{\mathbf{y}}^S|-|\vec{\mathbf{y}}|)}{2c_0}\right)\cos\left(\frac{\omega_0(|\vec{\mathbf{y}}^S|-|\vec{\mathbf{y}}|)}{c_0}\right)\widetilde{\mathcal{I}}^{\rm IF}(\vec{\mathbf{y}}^S)\,, \quad (44)$$

$$\widetilde{\mathcal{I}}^{\rm IF}(\vec{\mathbf{y}}^S)=\sum_{n=1}^{\infty}\frac{1}{\eta_c+\eta^n(\frac{\omega_0 a}{2c_0})}\phi^n\Big(\frac{\xi^S}{|\vec{\mathbf{y}}^S|},\frac{\omega_0 a}{2c_0}\Big)\phi^n\Big(\frac{\xi}{|\vec{\mathbf{y}}|},\frac{\omega_0 a}{2c_0}\Big)\,. \quad (45)$$

The hypothesis that B is small enough so that the eigenvalues and eigenvectors do not vary too much with the parameter $\omega a/(2c_0)$ for $\omega\in[\omega_0-B/2,\omega_0+B/2]$ is more stringent than the hypothesis that B is small enough so that we can approximate (33) by (35), because the eigenvalues and eigenvectors have strong variations with respect to their parameters. Therefore, if the bandwidth is not small enough, then one should consider the more complicated expression

$$\begin{aligned}\mathcal{I}^{\rm IF}(\vec{\mathbf{y}}^S)=\frac{1}{8\pi^2|\vec{\mathbf{y}}^S||\vec{\mathbf{y}}|}\cos\left(\frac{\omega_0(|\vec{\mathbf{y}}^S|-|\vec{\mathbf{y}}|)}{c_0}\right)\int_{-\frac{B}{2}}^{\frac{B}{2}}\sum_{n=1}^{N}\frac{1}{\eta_c+\eta^n(\frac{(\omega_0+\omega)a}{2c_0})}\\\times\phi^n\Big(\frac{\xi^S}{|\vec{\mathbf{y}}^S|},\frac{(\omega_0+\omega)a}{2c_0}\Big)\phi^n\Big(\frac{\xi}{|\vec{\mathbf{y}}|},\frac{(\omega_0+\omega)a}{2c_0}\Big)e^{i\frac{\omega}{c_0}(|\vec{\mathbf{y}}^S|-|\vec{\mathbf{y}}|)}d\omega\,. \quad (46)\end{aligned}$$

One can see from (44) that the range resolution is controlled by the bandwidth B, while the cross range (or angular) resolution is controlled by the carrier frequency ω_0 and the regularization number η_c. In particular,

- If we take a large regularization number η_c (i.e. much larger than one), then by using (C.4) we get that $\widetilde{\mathcal{I}}^{\rm IF}(\vec{\mathbf{y}}^S)$ defined by (45) becomes approximately:

$$\widetilde{\mathcal{I}}^{\rm IF}(\vec{\mathbf{y}}^S) \simeq \frac{1}{\eta_c}\sum_{n=1}^{\infty}\phi^n\Big(\frac{\xi^S}{|\vec{\mathbf{y}}^S|},\frac{\omega_0 a}{2c_0}\Big)\phi^n\Big(\frac{\xi}{|\vec{\mathbf{y}}|},\frac{\omega_0 a}{2c_0}\Big) = \frac{\omega_0 a}{2\pi c_0\eta_c}\mathrm{sinc}\left[\frac{\omega_0 a}{2c_0}\Big(\frac{\xi^S}{|\vec{\mathbf{y}}^S|}-\frac{\xi}{|\vec{\mathbf{y}}|}\Big)\right].$$

Since we should have $|\vec{\mathbf{y}}^S| \simeq |\vec{\mathbf{y}}|$ for the sinc term in (44) to be non-negligible, we get in these conditions

$$\widetilde{\mathcal{I}}^{\rm IF}(\vec{\mathbf{y}}^S) \simeq \frac{\omega_0 a}{2\pi c_0\eta_c}\mathrm{sinc}\left[\frac{\omega_0 a}{2c_0|\vec{\mathbf{y}}|}(\xi^S-\xi)\right], \tag{47}$$

which is like the KM functional (35). This shows that the cross range resolution $\lambda_0|\vec{\mathbf{y}}|/a$, which is the Rayleigh resolution formula obtained without applying the inverse filter (see Eq. (35)). Therefore, it is necessary to take a regularization number smaller than one in order to enhance cross range resolution.

- If we take $\eta_c \to 0$, then by using (C.5) we get that $\widetilde{\mathcal{I}}^{\rm IF}(\vec{\mathbf{y}}^S)$ becomes approximately:

$$\widetilde{\mathcal{I}}^{\rm IF}(\vec{\mathbf{y}}^S) \simeq \sum_{n=1}^{\infty}\frac{1}{\eta^n\big(\frac{\omega_0 a}{2c_0}\big)}\phi^n\Big(\frac{\xi^S}{|\vec{\mathbf{y}}^S|},\frac{\omega_0 a}{2c_0}\Big)\phi^n\Big(\frac{\xi}{|\vec{\mathbf{y}}|},\frac{\omega_0 a}{2c_0}\Big) = \delta\Big(\frac{\xi^S}{|\vec{\mathbf{y}}^S|}-\frac{\xi}{|\vec{\mathbf{y}}|}\Big). \tag{48}$$

This result shows that it is possible to improve refocusing dramatically, at the expense of SNR deterioration as we will see in the next section.

Remark: in the case in which $a/\lambda_0 \gg 1$, the behavior of the eigenvalues and eigenvectors is known (see Appendix C and [21]). The first $[2a/\lambda_0]$ eigenvalues are approximately equal to one, and the corresponding eigenvectors are of order one over the interval $[-1,1]$. The following eigenvalues plunge to zero as n increases, and the corresponding eigenvectors become concentrated at the edges ± 1. Therefore, if η_c is larger than one or of order one, then the IF imaging functional depends essentially only on the first $[2a/\lambda_0]$ pairs of eigenvalues/eigenvectors and it is basically like KM. As η_c becomes closer to zero, the IF imaging functional depends on more pairs of eigenvalues/eigenvectors.

7. Signal-to-noise ratio analysis in the continuum case

In this section we consider again passive imaging and assume that the sensors are along the segment $\vec{\mathbf{x}} \in [-a/2,a/2]\times\{0\}\times\{0\}$ and separated by $h \ll \lambda_0$. In the previous section we described passive imaging in the case of high (infinite) SNR. We now consider the case in which the SNR is finite. Here the SNR is defined as the ratio of the squared mean signal amplitude over the variance of the signal amplitude. We assume that the signals recorded by the array contain additive noise and have the form

$$\hat{P}(\vec{\mathbf{x}}_r,\omega) = \hat{G}(\vec{\mathbf{x}}_r,\vec{\mathbf{y}},\omega)\hat{f}(\omega) + \hat{\varepsilon}(x_r,\omega), \tag{49}$$

where $\vec{\mathbf{x}}_r = (x_r,0,0)$ and $\hat{\varepsilon}$ is the Fourier transform of a real-valued Gaussian process whose autocorrelation function is

$$\langle\varepsilon(x_r,t)\varepsilon(x_r',t')\rangle = \sigma^2 C_1\Big(\frac{x_r-x_r'}{l_c}\Big)C_2\Big(\frac{t-t'}{t_c}\Big)\mathbf{1}_{[0,T]}(t)\mathbf{1}_{[0,T]}(t').$$

It is the truncation over the recording time window $[0,T]$ of a zero-mean stationary Gaussian process. Here C_1 and C_2 are normalized so that $C_1(0)=1$, $C_2(0)=1$, $\hat{C}_1(0)=\int_{-\infty}^{\infty}C_1(x)dx=1$, and $\hat{C}_2(0)=\int_{-\infty}^{\infty}C_2(t)dt=1$. The quantities l_c and t_c are the correlation radius and the coherence time of the process ε. We assume in the following that $t_c \ll T$, so that

$$\Big\langle \hat{\varepsilon}(x_r,\omega)\overline{\hat{\varepsilon}(x_{r'},\omega')}\Big\rangle = \sigma^2 T t_c C_1\Big(\frac{x_r-x_r'}{l_c}\Big)\mathrm{sinc}\Big(\frac{T(\omega-\omega')}{2}\Big)\hat{C}_2\Big(\frac{t_c(\omega+\omega')}{2}\Big)e^{i\frac{T}{2}(\omega-\omega')}\,.$$

We also assume that $T > |\vec{\mathbf{y}}^S|/c$ for $\vec{\mathbf{y}}^S$ is the search window, which means that the sensor array records the signals over a time interval large enough to capture a signal emitted by a possible source in the search window, and $l_c \ll a$, which means that the additive noise has short-range spatial correlations.

7.1. SNR analysis for the KM imaging functional

We first perform the analysis in the Fourier domain and find

$$\begin{aligned}\mathrm{Cov}\Big(\hat{\mathcal{I}}^{\mathrm{KM}}(\vec{\mathbf{y}}^S,\omega),\overline{\hat{\mathcal{I}}^{\mathrm{KM}}}(\vec{\mathbf{y}}^S,\omega')\Big) &= \sum_{r,r'=1}^{N}\hat{G}(\vec{\mathbf{y}}^S,\vec{\mathbf{x}}_r,\omega)\overline{\hat{G}(\vec{\mathbf{y}}^S,\vec{\mathbf{x}}_{r'},\omega')}\,\Big\langle\overline{\hat{\varepsilon}(x_r,\omega)}\hat{\varepsilon}(x_{r'},\omega')\Big\rangle \\ &= \frac{\sigma^2 T t_c l_c a}{16\pi^2 h^2|\vec{\mathbf{y}}^S|^2}\mathrm{sinc}\Big(\frac{T(\omega-\omega')}{2}\Big)\hat{C}_2\Big(\frac{t_c(\omega+\omega')}{2}\Big)e^{i(\frac{|\vec{\mathbf{y}}^S|}{c_0}-\frac{T}{2})(\omega-\omega')}\,. \qquad (50)\end{aligned}$$

Next we return to the time domain. We first show that it is possible to reduce the noise level by filtering the recorded signals. If the recorded signals are not filtered, then

$$\mathrm{Var}\big(\mathcal{I}^{\mathrm{KM}}(\vec{\mathbf{y}}^S)\big) = \frac{1}{4\pi^2}\int_{-\infty}^{\infty}\int_{-\infty}^{\infty}\mathrm{Cov}\Big(\hat{\mathcal{I}}^{\mathrm{KM}}(\vec{\mathbf{y}}^S,\omega),\overline{\hat{\mathcal{I}}^{\mathrm{KM}}}(\vec{\mathbf{y}}^S,\omega')\Big)\,d\omega d\omega'\,,$$

and we obtain

$$\mathrm{Var}\big(\mathcal{I}^{\mathrm{KM}}(\vec{\mathbf{y}}^S)\big) = \frac{\sigma^2 l_c a}{16\pi^2 h^2|\vec{\mathbf{y}}^S|^2}\mathbf{1}_{(0,T)}\Big(\frac{|\vec{\mathbf{y}}^S|}{c_0}\Big) = \frac{\sigma^2 l_c a}{16\pi^2 h^2|\vec{\mathbf{y}}^S|^2}\,. \qquad (51)$$

If we filter the recorded signals to keep only the frequency bands $[\omega_0-B/2,\omega_0+B/2]$ and $[-\omega_0-B/2,-\omega_0+B/2]$, which are the support of the source, and if we assume that $\omega_0 t_c \ll 1$ and $BT>1$, that is, we assume that the coherence time of the additive noise times the propagation speed is shorter than the carrier wavelength, and the recording time window is longer than the pulse width, which is natural, then we get

$$\mathrm{Var}\big(\mathcal{I}^{\mathrm{KM}}(\vec{\mathbf{y}}^S)\big) = \frac{\sigma^2 l_c a t_c B}{16\pi^3 h^2|\vec{\mathbf{y}}^S|^2}\,. \qquad (52)$$

This second expression of the variance is smaller than the previous one, by the factor $t_c B/\pi$, because we have integrated only over two frequency bands of length B which is smaller than the length of the frequency band of the noise, which is of order $1/t_c$.

Note that the variance of the KM imaging functional is constant when $\vec{\mathbf{y}}^S$ is taken over the sphere of radius L. Using the fact that the mean KM imaging functional is (35), we obtain that the output SNR is

$$\mathrm{SNR}_{\mathrm{KM}} = \frac{a}{16\pi|\vec{\mathbf{y}}^S|^2\sigma^2 l_c B t_c}\,. \qquad (53)$$

Since the input SNR is

$$\mathrm{SNR_i} = \frac{1}{16\pi^2 |\vec{\mathbf{y}}^S|^2 \sigma^2}\,, \tag{54}$$

we obtain that

$$\mathrm{SNR_{KM}} = \frac{\pi a}{l_c B t_c} \mathrm{SNR_i}\,. \tag{55}$$

As it could be expected, the SNR is large when the array is large (compared to the correlation radius of the noise) and when the pulse width if large (compared to the coherence time of the noise).

7.2. SNR analysis for the IF imaging functional

We find in the Fourier domain

$$\begin{aligned}\mathrm{Cov}\left(\hat{\mathcal{I}}^{\mathrm{IF}}(\vec{\mathbf{y}}^S,\omega), \overline{\hat{\mathcal{I}}^{\mathrm{IF}}}(\vec{\mathbf{y}}^S,\omega')\right) &= \frac{\sigma^2 T t_c l_c}{8\pi^3 |\vec{\mathbf{y}}^S|^2} \mathrm{sinc}\Big(\frac{T(\omega-\omega')}{2}\Big) \hat{C}_2\Big(\frac{t_c(\omega+\omega')}{2}\Big) e^{i(\frac{|\vec{\mathbf{y}}^S|}{c_0} - \frac{T}{2})(\omega-\omega')} \\ &\quad \times \left(\frac{\omega}{c_0} \sum_{n=1}^{\infty} \frac{1}{\left(\eta_c + \eta^n(\frac{\omega a}{2c_0})\right)^2} \phi^n\Big(\frac{\xi^S}{|\vec{\mathbf{y}}^S|}, \frac{\omega a}{2c_0}\Big)^2\right), \end{aligned} \tag{56}$$

and in the time domain

$$\mathrm{Var}\left(\mathcal{I}^{\mathrm{IF}}(\vec{\mathbf{y}}^S)\right) = \frac{\sigma^2 \omega_0 B t_c l_c}{8\pi^4 c_0 |\vec{\mathbf{y}}^S|^2} \left(\sum_{n=1}^{\infty} \frac{1}{\left(\eta_c + \eta^n(\frac{\omega_0 a}{2c_0})\right)^2} \phi^n\Big(\frac{\xi^S}{|\vec{\mathbf{y}}^S|}, \frac{\omega_0 a}{2c_0}\Big)^2\right). \tag{57}$$

As in the previous subsection, we have filtered the time signals to retain only the frequency bands $[-\omega_0 - B/2, -\omega_0 + B/2]$ and $[\omega_0 - B/2, \omega_0 + B/2]$. Note that the variance depends on $\xi^S/|\vec{\mathbf{y}}^S|$, in contrast to the KM case. We have also assumed that the bandwidth B is smaller than the carrier frequency ω_0, so that the eigenvalues and eigenvectors do not vary too much with the parameter $\omega a/(2c_0)$ for ω in the source bandwidth.

In the case in which we take η_c larger than or of the order of one, by using (C.4) we get that the variance is

$$\mathrm{Var}\left(\mathcal{I}^{\mathrm{IF}}(\vec{\mathbf{y}}^S)\right) \sim \frac{\omega_0 \sigma^2 B t_c l_c}{8\pi^4 c_0 |\vec{\mathbf{y}}^S|^2 \eta_c^2} \frac{\omega_0 a}{2\pi c_0} = \frac{\sigma^2 B t_c \omega_0^2 l_c a}{16\pi^5 c_0^2 |\vec{\mathbf{y}}^S|^2 \eta_c^2}\,.$$

In the case in which we take η_c smaller than one, in order to improve resolution, the expression of the variance incorporates more and more pairs of eigenvalues/eigenvectors. The variance is then large, and especially in the regions where $|\xi^S| \ll |\vec{\mathbf{y}}^S|$, that is, the points close to the axis of the sensor array.

Taking into account the expression (44) of the mean IF imaging functional, the output SNR is

$$\mathrm{SNR_{IF}} = \frac{2\pi^2 c_0}{\omega_0 l_c B t_c} \frac{\left(\sum_{n=1}^{\infty} \frac{1}{\eta_c + \eta^n\left(\frac{\omega_0 a}{2c_0}\right)} \phi^n\left(\frac{\xi^S}{|\vec{\mathbf{y}}^S|}, \frac{\omega_0 a}{2c_0}\right) \phi^n\left(\frac{\xi}{|\vec{\mathbf{y}}|}, \frac{\omega_0 a}{2c_0}\right)\right)^2}{\left(\sum_{n=1}^{\infty} \frac{1}{\left(\eta_c + \eta^n\left(\frac{\omega_0 a}{2c_0}\right)\right)^2} \phi^n\left(\frac{\xi^S}{|\vec{\mathbf{y}}^S|}, \frac{\omega_0 a}{2c_0}\right)^2\right)} \mathrm{SNR_i}\,. \tag{58}$$

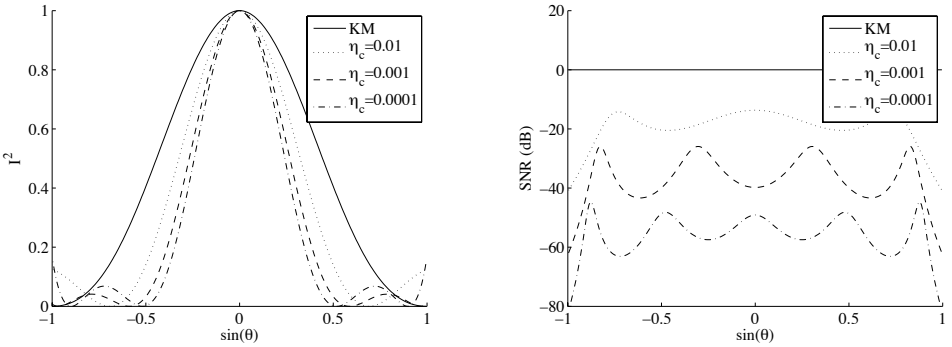

Figure 8. Imaging functional and SNR as a function of the position $x = L\sin(\theta)$ and $z = L\cos(\theta)$. The point source is located at $x = 0$ and $z = L$ and it emits a narrowband pulse ($B = 0.01$).

If $\eta_c > 1$, then

$$\mathrm{SNR_{IF}} \simeq \frac{2\pi^2 c_0}{\omega_0 l_c B t_c}\frac{\omega_0 a}{2\pi c_0}\mathrm{SNR_i} = \frac{\pi a}{l_c B t_c}\mathrm{SNR_i} = \mathrm{SNR_{KM}}\,.$$

Therefore, by taking η_c larger than one, we recover the result of the KM functional, both in terms of resolution and SNR.

If $\eta_c < 1$, then the resolution is improved compared to KM, but the SNR is also reduced.

7.3. Numerical illustrations

In this subsection we plot the theoretical KM and IF imaging functionals and SNRs in the case in which $a = \lambda_0 = c_0 = 1$. We study the impact of the choice of the regularization number η_c.

We first consider a narrowband case (Figures 8-10). We can see that it is possible to get a better resolution than the one obtained with KM when taking a small value for η_c. However, the SNR is reduced as well, and it is fluctuating with the position. For $\eta_c = 10^{-2}$ the SNR reduction is 15 dB and the resolution is enhanced by 27% (the full-width at half maximum is reduced by 27%). For $\eta_c = 10^{-3}$ the SNR reduction is 39 dB and the resolution is enhanced by 40%.

Next we consider a broadband case (Figures 11-12). We can observe that the SNR as a function of the position is almost constant, except close to the edges (i.e. close to the axis of the array), and that the sidelobes are reduced, compared to the results obtained in the narrowband case. The efficiency in terms of resolution enhancement is very similar to the narrowband case.

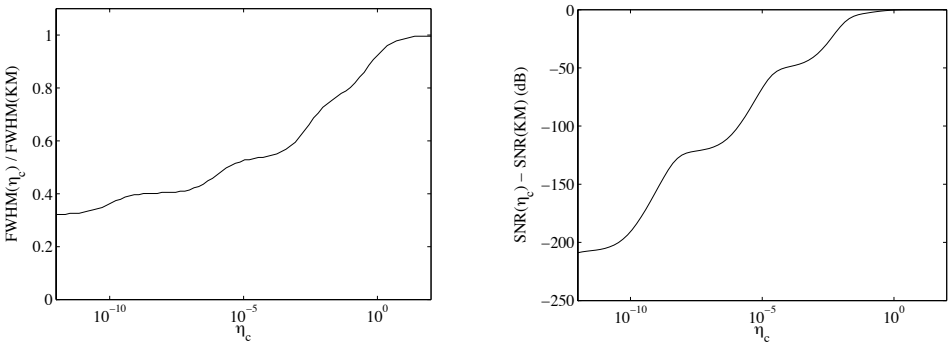

Figure 9. Resolution enhancement (ratio of the full width at half maximum) and SNR reduction at the center of the image for the configuration of Figure 8 .

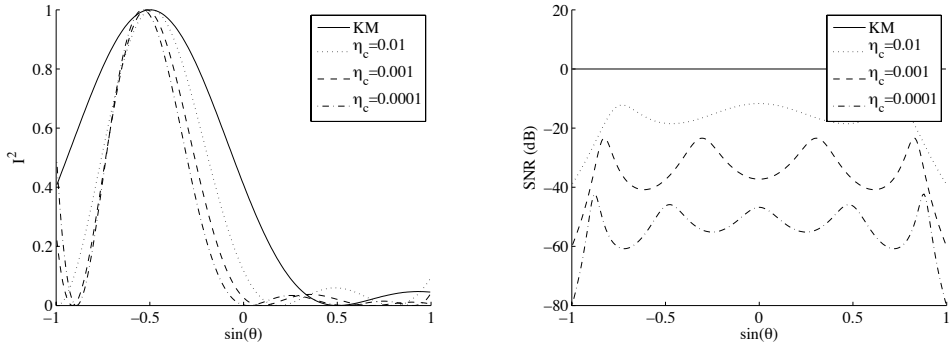

Figure 10. Imaging functional and SNR. The point source is located at $x = -L/\sqrt{2}$ and $z = L/\sqrt{2}$ and it emits a narrowband pulse ($B = 0.01$).

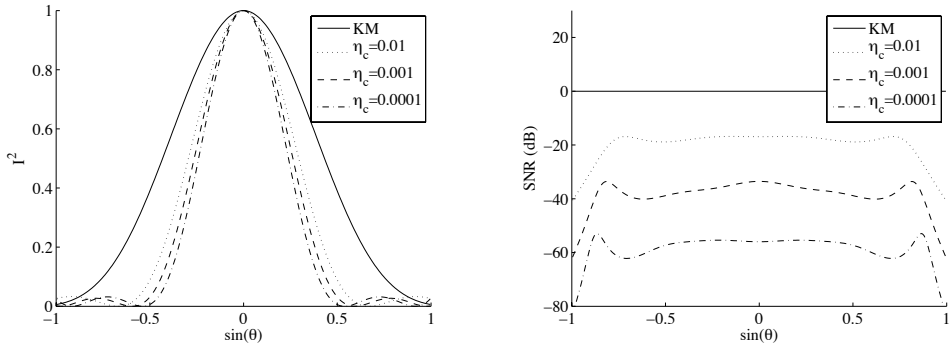

Figure 11. Imaging functional and SNR as a function of the position $x = L\sin(\theta)$ and $z = L\cos(\theta)$. The point source is located at $x = 0$ and $z = L$ and it emits a broadband pulse ($B = 1$).

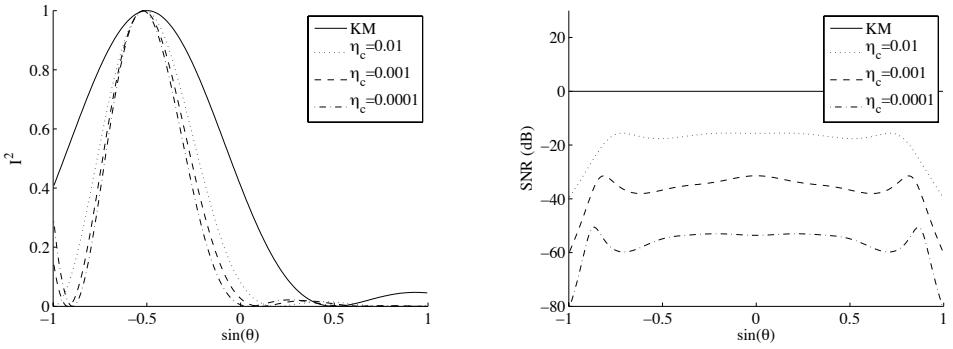

Figure 12. Imaging functional and SNR. The point source is located at $x = -L/\sqrt{2}$ and $z = L/\sqrt{2}$ and it emits a broadband pulse ($B = 1$).

8. SNR issues in passive imaging for a discrete array

In this section we give a general analysis of the SNR of the imaging methods based on the use of the inverse filter on the one hand and on standard KM on the other hand in the case of a general discrete array of point sensors. In particular, we give in Subsection 8.3 a practical way to choose the regularization number μ_c^ω.

8.1. Frequency domain

We assume that the signals recorded by the discrete array $\{\vec{\mathbf{x}}_r, r = 1, \dots, N\}$ contain additive noise and have the form

$$\hat{P}(\vec{\mathbf{x}}_r, \omega) = \hat{G}(\vec{\mathbf{x}}_r, \vec{\mathbf{y}}, \omega)\hat{f}(\omega) + \hat{\varepsilon}_r(\omega)\,, \tag{59}$$

where $\hat{\varepsilon}_r(\omega)$, $r = 1, \dots, N$, are independent complex Gaussian random variables with zero mean and variance σ_ω^2. The input SNR is

$$\mathrm{SNR}_{\mathrm{i}}^\omega = \frac{|\hat{f}(\omega)|^2}{16\pi^2|\vec{\mathbf{y}}|^2\sigma_\omega^2}\,. \tag{60}$$

In these conditions, the first two moments of the KM imaging functional are

$$\Big\langle \hat{\mathcal{I}}^{\mathrm{KM}}(\vec{\mathbf{y}}^S = \vec{\mathbf{y}}, \omega)\Big\rangle = \frac{N\overline{\hat{f}(\omega)}}{16\pi^2|\vec{\mathbf{y}}|^2}\,, \quad \mathrm{Var}\Big(\hat{\mathcal{I}}^{\mathrm{KM}}(\vec{\mathbf{y}}^S, \omega)\Big) = \frac{N\sigma_\omega^2}{16\pi^2|\vec{\mathbf{y}}^S|^2}\,, \tag{61}$$

so that the output SNR (i.e. the one of the refocused wavefield) is

$$\mathrm{SNR}_{\mathrm{KM}}^\omega = N\,\mathrm{SNR}_{\mathrm{i}}^\omega\,. \tag{62}$$

The moments of the IF imaging functional are

$$\Big\langle \hat{\mathcal{I}}^{\mathrm{IF}}(\vec{\mathbf{y}}^S = \vec{\mathbf{y}}, \omega)\Big\rangle = \frac{\overline{\hat{f}(\omega)}}{16\pi^2|\vec{\mathbf{y}}|^2}\sum_{n=1}^N \frac{|\hat{c}_n(\vec{\mathbf{y}}, \omega)|^2}{\mu_c^\omega + \mu^n(\omega)}\,, \tag{63}$$

$$\mathrm{Var}\Big(\hat{\mathcal{I}}^{\mathrm{IF}}(\vec{\mathbf{y}}^S, \omega)\Big) = \frac{1}{16\pi^2|\vec{\mathbf{y}}^S|^2}\sum_{n=1}^N \frac{|\hat{c}_n(\vec{\mathbf{y}}^S, \omega)|^2\sigma_\omega^2}{\left(\mu_c^\omega + \mu^n(\omega)\right)^2}\,, \tag{64}$$

where

$$\hat{c}_n(\vec{\mathbf{y}}^S,\omega) = 4\pi|\vec{\mathbf{y}}^S|\sum_{r=1}^N \psi_r^n(\omega)\hat{G}(\vec{\mathbf{x}}_r,\vec{\mathbf{y}}^S,\omega) = \sum_{r=1}^N \psi_r^n(\omega)e^{i\frac{\omega}{c_0}|\vec{\mathbf{x}}_r-\vec{\mathbf{y}}|}\,,$$

so that the output SNR is

$$\mathrm{SNR}_{\mathrm{IF}}^{\omega} = \frac{\left(\sum_{n=1}^N \frac{|\hat{c}_n(\vec{\mathbf{y}},\omega)|^2}{\mu_c^\omega+\mu^n(\omega)}\right)^2}{\sum_{n=1}^N \frac{|\hat{c}_n(\vec{\mathbf{y}},\omega)|^2}{\left(\mu_c^\omega+\mu^n(\omega)\right)^2}}\,\mathrm{SNR}_{\mathrm{i}}^{\omega}\,. \tag{65}$$

These formulas (valid for a fixed frequency) are used in the next subsection to determine the SNRs of the two methods for regularly sampled signals in the time domain.

8.2. Time domain

The previous calculations consider SNR issues in the time-harmonic case, assuming that the noises recorded at each sensor are independent with variance σ_ω^2. In a real experiment, the signals are recorded in the time domain. More precisely, the recorded signal $P(\vec{\mathbf{x}}_r,t)$ at the rth element of the sensor array is sampled over the time interval $[0,T]$ at frequency M/T, and each measure is noisy:

$$p_{r,m} := P\Big(\vec{\mathbf{x}}_r,\frac{mT}{M}\Big) = \Big[G(\vec{\mathbf{x}}_r,\vec{\mathbf{y}},\cdot)*f\Big]\Big(\frac{mT}{M}\Big)+\varepsilon_{r,m},\quad r=1,\dots,N,\quad m=0,\dots,M-1.$$

The errors $(\varepsilon_{r,m})_{r=1,\dots,N,\,m=0,\dots,M-1}$, are real independent Gaussian random variables with variance σ^2. A simple estimate of the SNR in the case of a regularly sampled linear array can be obtained by noting that this situation can be seen as a discretized version of the continuous case in which the correlation radius of the noise is $l_c = a/N$ (the step of the array) and $t_c = T/M$ (the time step of the recording window). A more detailed analysis can be performed as follows.

The signal is analyzed by discrete Fourier transform

$$\hat{p}_{r,j} = \sum_{m=0}^{M-1} p_{r,m}e^{i2\pi\frac{jm}{M}},\quad r=1,\dots,N,\quad j=0,\dots,M-1.$$

If $M/T \geq \omega_0 \gg B$, then

$$\hat{p}_{r,j} \simeq \frac{M}{T}\Big[\hat{G}\Big(\vec{\mathbf{x}}_r,\vec{\mathbf{y}},j\frac{2\pi}{T}\Big)\hat{f}\Big(j\frac{2\pi}{T}\Big)+\hat{G}\Big(\vec{\mathbf{x}}_r,\vec{\mathbf{y}},(M-j)\frac{2\pi}{T}\Big)\hat{f}\Big((M-j)\frac{2\pi}{T}\Big)\Big]+\hat{\varepsilon}_{r,j}\,,$$

where

$$\hat{\varepsilon}_{r,j} = \sum_{m=0}^{M-1}\varepsilon_{r,m}e^{i2\pi\frac{jm}{M}},\quad r=1,\dots,N,\quad j=0,\dots,M-1,$$

is a collection of independent complex Gaussian random variables with variance $\sigma_\omega^2 = \sigma^2 M$.

There are about

- $\frac{4\pi M}{BT}$ points in the support of the mean recorded signal in the time domain,

• $2 \times \frac{BT}{2\pi}$ points in the support of the mean recorded signal in the frequency domain.

These estimates are based on the case (34).

The signal amplitude in the time domain is 1, while the noise variance is σ^2. Therefore the input SNR is

$$\mathrm{SNR}_{\mathrm{i}}^t = \frac{1}{\sigma^2}\,.$$

The signal amplitude in the frequency domain is $\frac{M}{T}\frac{2\pi}{B}$, while the noise variance is $\sigma_\omega^2 = \sigma^2 M$. Therefore the input SNR at frequency ω is

$$\mathrm{SNR}_{\mathrm{i}}^\omega = \frac{4\pi^2 M}{B^2T^2\sigma^2} = \frac{4\pi^2 M}{B^2T^2}\mathrm{SNR}_{\mathrm{i}}^t\,.$$

For each frequency, the SNR of the KM method and the IF method is given by (62) and (65). There are $\frac{BT}{2\pi}$ discrete frequencies (around ω_0) in the bandwidth, with independent noise components. If the time signals are filtered to retain only this frequency band, then there is no other noise component and the SNR of the KM method in the time domain is

$$\mathrm{SNR}_{\mathrm{KM}}^t = \frac{BT}{\pi}\mathrm{SNR}_{\mathrm{KM}}^{\omega_0} = \frac{NBT}{\pi}\mathrm{SNR}_i^{\omega_0} = \frac{4\pi MN}{BT}\,\mathrm{SNR}_{\mathrm{i}}^t\,,$$

and the one of the IF method is (assuming $B \ll \omega_0$ so that the ratio $\mathrm{SNR}_{\mathrm{IF}}^\omega/\mathrm{SNR}_{\mathrm{i}}^\omega$ given by (65) does not vary too much over the bandwidth)

$$\mathrm{SNR}_{\mathrm{IF}}^t = \frac{BT}{\pi}\mathrm{SNR}_{\mathrm{IF}}^{\omega_0} = \frac{\pi M}{BT}\frac{\left(\sum_{n=1}^N \frac{|\hat{c}_n(\omega_0,\vec{\mathbf{y}})|^2}{\mu_c^{\omega_0}+\mu^n(\omega_0)}\right)^2}{\sum_{n=1}^N \frac{|\hat{c}_n(\omega_0,\vec{\mathbf{y}})|^2}{\left(\mu_c^{\omega_0}+\mu^n(\omega_0)\right)^2}}\,\mathrm{SNR}_{\mathrm{i}}^t\,.$$

These two results are in agreement with the analysis of the continuum case (see (55) and (58)), with the equivalence $t_c = T/M$ and $l_c = a/N$. For both methods, compared to the time-harmonic case, the SNR in the time domain is enhanced by the factor

$$\frac{\mathrm{SNR}^t}{\mathrm{SNR}^\omega} = \frac{\pi M}{BT}\,, \tag{66}$$

which is proportional to the ratio of the sampling frequency M/T over the bandwidth B.

8.3. Determination of the regularization number μ_c^ω

We finally discuss the practical choice of the regularization number μ_c^ω. As pointed out before, it can be a frequency-dependent number, but the resolution of the general optimization problem for a general frequency-dependent regularization number is complicated, so we first first simplify the optimization problem. Motivated by the scaling (37) of the eigenvalues μ_n in terms of the dimensionless eigenvalues η_n, we see that the regularization number should scale as $1/\omega$. Therefore we will look for the optimal frequency-dependent regularization number μ_c^ω in the form

$$\mu_c^\omega = \frac{\omega_0}{\omega}\mu_c\,,$$

where ω_0 is the carrier frequency and μ_c is the frequency-independent regularization number to be determined by the optimization algorithm. This regularization number should be chosen as small as possible (to enhance resolution), but beyond a threshold value so that the obtained image is not noisy. In Figure 3 and 5, one plots several images and we obtain empirically that $\mu_c = 10^{-3}$ achieves a reasonable trade-off between resolution and SNR in this situation.

The idea is now to develop an adaptive algorithm that determines the optimal parameter μ_c as a function of the data. For this, one needs to define a search domain $\mathcal{D}$ (for instance the domain $[-350, 350]\times[75, 375]$ plotted in Figures 3 and 5) and a norm for the image obtained with a given regularization number that measures its quality, both in terms of resolution and SNR. This trade-off is usual in spectral estimation of time series [18] or in image processing [10]. This norm should penalize speckle fluctuations and it should minimize blurring. We have examined different algorithms, in particular the ones proposed in [7], and it turns out that the L^2 norm of the normalized imaging functional performs well. The algorithm for a general L^p-norm is the following one.

L^p-algorithm: for any given μ_c, calculate the normalized imaging functional

$$\mathcal{K}(\vec{\mathbf{y}}^S;\mu_c) = \frac{\mathcal{I}(\vec{\mathbf{y}}^S;\mu_c)}{\sup_{\vec{\mathbf{y}}^{S'}\in\mathcal{D}} |\mathcal{I}(\vec{\mathbf{y}}^{S'};\mu_c)|}\,,$$

and choose the regularization number $\mu_c^{(p)}$ minimizing

$$\mathcal{N}_p(\mu_c) = \|\mathcal{K}(\vec{\mathbf{y}}^S;\mu_c)\|_{L^p(\mathcal{D})}\,. \tag{67}$$

We have observed (but not rigorously proved) that the function $\mathcal{N}_p(\mu_c)$ presents a unique minimum. This can be understood as follows. Let us start from a large value of μ_c. When μ_c decays, resolution is enhanced and noise is not yet noticeable (see Figure 2 for instance). Therefore, the contributions of the main peak(s) to the function $\mathcal{N}_p(\mu_c)$ decays and the L^p-norm of the image decays. However, for small values of μ_c, noise appears in the image, in the form of speckle. The value of the function $\mathcal{N}_p(\mu_c)$ is reduced by the resolution enhancement of the main peak(s), but increased by the contributions of the speckle. Below a critical value, resolution enhancement is overwhelmed by the speckle and the L^p-norm of the image increases. We have also studied the role of the parameter p. If p is small, then the noise of the image obtained with $\mu_c^{(p)}$ is very low, but the image is oversmoothed. If p is large, then the resolution is very good but the image is noisy. The choice $p = 2$ achieves the optimal trade-off between resolution and SNR in all configurations studied in this paper (see Figure 13).

9. Summary and Conclusions

In this paper we show that it is possible to use a universal filter to achieve cross range resolution enhancement in imaging with small arrays, in homogeneous media. We first studied the least squares problem that gives the form of the inverse filter. It maximizes the peak of the imaging functional on the target point and minimizes it at a set of

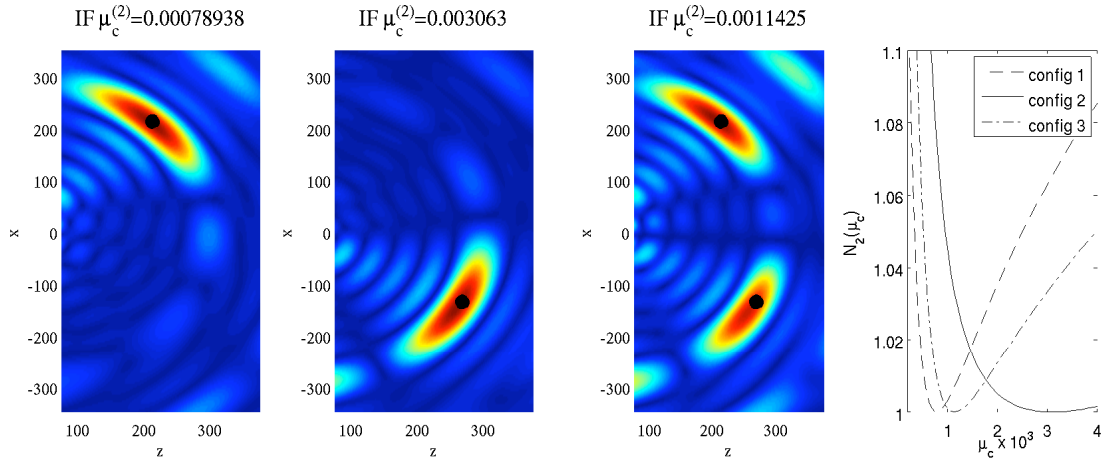

Figure 13. Optimal images obtained in three different configurations (one or two point targets) with the L^2-minimization algorithm.

control points. We then noted that the inverse filter acquires a universal form when the control array is a surface that encloses the sensor array and is in the far field region. The inverse filter method is the KM method when the sensors on the array are placed the Nyquist spatial frequency, as noted in [27]. However, when the array sensors are placed in an oversampled pattern, then cross range resolution can be increased at the expense of some loss in SNR. We have analyzed carefully the trade-off between cross range resolution enhancement and SNR degradation.

The IF method described in this paper is useful for imaging but it may not be so useful in time-reversal wave focusing or antenna beamforming where the back propagation is a physical process. Application of the inverse filter requires amplification of the recorded signals that may not be compatible with the physical limitations on the maximal power radiated by an antenna. In imaging, back propagation is done numerically, and the limitations are in terms of SNR.

The IF method is useful in configurations in which the physical size of the array is small and has many sensors assembled beyond the Nyquist spatial sampling rate. This paper shows that one can make use of this oversampling for enhanced imaging resolution in homogeneous media. The generalization of this work to heterogeneous media requires the analysis of the random matrix $\mathcal{G}^\star\mathcal{G}$, which is related to the backscattering matrix from the sensor array to itself.

Acknowledgments

The work of G. Papanicolaou and T. Callaghan was partially supported by US Army grant W911NF-07-2-0027-1, ONR grant N00014-02-1-0088, and AFOSR grant FA9550-08-1-0089. The work of L. Borcea was partially supported by the Office of Naval Research, under grant N00014-05-1-0699 and by the National Science Foundation, grants

DMS-0604008, DMS-0305056, DMS-0354658.

Appendix A. Derivation of the inverse filter kernel (26)

We first give a direct derivation of the expression (26) for the kernel of the inverse filter when the control array is the surface of a sphere of radius L with center at $\mathbf{0}$, $\partial B(\mathbf{0}, L)$.

The LS filter is the inverse of

$$(\mathcal{G}^\star(\omega)\mathcal{G}(\omega))_{rr'} = \sum_{q=1}^{N_q} \frac{1}{16\pi^2|\vec{\mathbf{x}}_r - \vec{\mathbf{y}}_q||\vec{\mathbf{x}}_{r'} - \vec{\mathbf{y}}_q|} e^{i\frac{\omega}{c_0}(|\vec{\mathbf{x}}_{r'}-\vec{\mathbf{y}}_q|-|\vec{\mathbf{x}}_r-\vec{\mathbf{y}}_q|)} .$$

If the control surface is far from the sensor array so that $a \ll L$ and $(\omega/c_0)a^2 \ll L$, where a is the diameter of the sensor array, then

$$(\mathcal{G}^\star(\omega)\mathcal{G}(\omega))_{rr'} = \sum_{q=1}^{N_q} \frac{1}{16\pi^2|\vec{\mathbf{y}}_q|^2} e^{i\frac{\omega\vec{\mathbf{y}}_q\cdot(\vec{\mathbf{x}}_r-\vec{\mathbf{x}}_{r'})}{c_0|\vec{\mathbf{y}}_q|}} .$$

Since the control array is taken to be the continuum of points on $\partial B(\mathbf{0}, L)$, we have

$$(\mathcal{G}^\star(\omega)\mathcal{G}(\omega))_{rr'} = \frac{N_q}{4\pi L^2} \int_{\partial B(\mathbf{0},L)} \frac{1}{16\pi^2|\vec{\mathbf{y}}|^2} e^{i\frac{\omega\vec{\mathbf{y}}\cdot(\vec{\mathbf{x}}_r-\vec{\mathbf{x}}_{r'})}{c_0|\vec{\mathbf{y}}|}} dS(\vec{\mathbf{y}}) .$$

After the change of variables $\vec{\mathbf{y}} = L\vec{\mathbf{z}}$ we have

$$(\mathcal{G}^\star(\omega)\mathcal{G}(\omega))_{rr'} = \frac{N_q}{64\pi^3 L^2} \int_{\partial B(\mathbf{0},1)} e^{i\frac{\omega}{c_0}\vec{\mathbf{z}}\cdot(\vec{\mathbf{x}}_r-\vec{\mathbf{x}}_{r'})} dS(\vec{\mathbf{z}}) .$$

The integration can be carried out in polar coordinates and we obtain

$$(\mathcal{G}^\star(\omega)\mathcal{G}(\omega))_{rr'} = \frac{N_q}{16\pi^2 L^2} \mathrm{sinc}\Big(\frac{\omega}{c_0}|\vec{\mathbf{x}}_r - \vec{\mathbf{x}}_{r'}|\Big) .$$

We get (26) by taking N_q proportional to the surface of the sphere $\partial B(\mathbf{0}, L)$.

We now give a more general derivation of the kernel (26) which does not require a homogeneous medium. We assume that (i) the background medium can be smoothly varying around the array but must be homogeneous (with background velocity c_e) outside a ball $B(\mathbf{0}, D)$ enclosing the imaging array (ii) the control surface $\partial B(\mathbf{0}, L)$ is far from the array in the sense that $L \gg D$. By smoothly varying we mean that the index of refraction does not change significantly over distances comparable to wavelengths in the bandwidth. If $\hat{G}(\vec{\mathbf{x}}, \vec{\mathbf{y}}, \omega)$ denotes the outgoing, time harmonic Green's function

$$\Delta_{\vec{\mathbf{y}}}\hat{G}(\vec{\mathbf{x}}, \vec{\mathbf{y}}, \omega) + \frac{\omega^2}{c^2(\vec{\mathbf{y}})}\hat{G}(\vec{\mathbf{x}}, \vec{\mathbf{y}}, \omega) = -\delta(\vec{\mathbf{y}} - \vec{\mathbf{x}}),$$

then by using the second Green's identity we get

$$\int_{\partial B(\mathbf{0},L)} \mathbf{n}(\vec{\mathbf{y}}) \cdot \Big[\overline{\hat{G}(\vec{\mathbf{x}}_r, \vec{\mathbf{y}}, \omega)}\nabla_{\vec{\mathbf{y}}}\hat{G}(\vec{\mathbf{x}}_{r'}, \vec{\mathbf{y}}, \omega) - \hat{G}(\vec{\mathbf{x}}_{r'}, \vec{\mathbf{y}}, \omega)\nabla_{\vec{\mathbf{y}}}\overline{\hat{G}(\vec{\mathbf{x}}_r, \vec{\mathbf{y}}, \omega)}\Big] dS(\vec{\mathbf{y}})$$
$$= \hat{G}(\vec{\mathbf{x}}_r, \vec{\mathbf{x}}_{r'}, \omega) - \overline{\hat{G}(\vec{\mathbf{x}}_r, \vec{\mathbf{x}}_{r'}, \omega)} ,$$

where $\mathbf{n}(\vec{\mathbf{y}}) = \vec{\mathbf{y}}/|\vec{\mathbf{y}}|$ is the outward normal to the surface. Applying the Sommerfeld radiation condition, which is valid under hypotheses (i) and (ii) for $\vec{\mathbf{y}}$ on $\partial B(\mathbf{0}, L)$, we obtain the Kirchhoff-Helmholtz identity

$$\frac{2i\omega}{c_e}\int_{\partial B(\mathbf{0},L)} \overline{\hat{G}(\vec{\mathbf{x}}_{r'},\vec{\mathbf{y}},\omega)}\hat{G}(\vec{\mathbf{x}}_r,\vec{\mathbf{y}},\omega)dS(\vec{\mathbf{y}}) = \hat{G}(\vec{\mathbf{x}}_r,\vec{\mathbf{x}}_{r'},\omega) - \overline{\hat{G}(\vec{\mathbf{x}}_r,\vec{\mathbf{x}}_{r'},\omega)}\,. \tag{A.1}$$

This identity is well known in homogeneous meda, [5, p. 473] and [9, p. 419], and also when the medium is heterogeneous, [29]. Since the control array is taken to be the continuum of points on $\partial B(\mathbf{0}, L)$, we have

$$(\mathcal{G}^\star(\omega)\mathcal{G}(\omega))_{rr'} = \int_{\partial B(\mathbf{0},L)} \overline{\hat{G}(\vec{\mathbf{x}}_r,\vec{\mathbf{y}},\omega)}\hat{G}(\vec{\mathbf{x}}_{r'},\vec{\mathbf{y}},\omega)dS(\vec{\mathbf{y}})\,.$$

The Kirchhoff-Helmholtz identity (A.1) gives that the right side is approximately equal to the sinc kernel (26) with c_0 the constant background speed in the vicinity of the sensor array. This is because in this case

$$\hat{G}(\vec{\mathbf{x}}_r,\vec{\mathbf{x}}_{r'},\omega) \approx \frac{e^{i\frac{\omega}{c_0}|\vec{\mathbf{x}}_r-\vec{\mathbf{x}}_{r'}|}}{4\pi|\vec{\mathbf{x}}_r-\vec{\mathbf{x}}_{r'}|}.$$

Appendix B. Optimal refocusing for active imaging

In this appendix we discuss the choice of the filter $\hat{K}$ so as to optimize refocusing in the active imaging configuration. We consider active array imaging where the object to be imaged is a reflector that is small compared to the wavelength. We also assume that there is no noise and that the Born approximation is valid [9], that is, we take into account only single scattering by the reflector that we want to image. Then the impulse response matrix has the form

$$\hat{\Pi}(\vec{\mathbf{x}}_r,\vec{\mathbf{x}}_s,\omega) = \hat{G}(\vec{\mathbf{x}}_r,\vec{\mathbf{y}},\omega)\Xi_{\vec{\mathbf{y}}}\hat{G}(\vec{\mathbf{y}},\vec{\mathbf{x}}_s,\omega)\,, \quad r,s = 1,\ldots,N\,,$$

where $\Xi_{\vec{\mathbf{y}}}$ is the scattering amplitude of the reflector located at $\vec{\mathbf{y}}$, and the signals recorded by the array are

$$\hat{P}(\vec{\mathbf{x}}_r,\vec{\mathbf{x}}_s,\omega) = \hat{\Pi}(\vec{\mathbf{x}}_r,\vec{\mathbf{x}}_s,\omega)\hat{f}(\vec{\mathbf{x}}_s,\omega)\,, \quad r,s = 1,\ldots,N\,,$$

where $\hat{f}(\vec{\mathbf{x}}_s,\omega)$ is the illumination. For simplicity we assume a uniform illumination of the form:

$$\hat{f}(\vec{\mathbf{x}}_s,\omega) = \hat{f}(\omega) \quad \forall s = 1,\ldots,N\,. \tag{B.1}$$

In order to characterize the quality of the refocusing, we consider that the reflector position belongs to the control array $\{\vec{\mathbf{y}}_q, q = 1,\ldots,N_q\}$. We wish to find a kernel that permits the best refocusing on this array. That is to say, if $\vec{\mathbf{y}}_{q_0}$ is the position of the reflector, then we wish that the imaging functional refocuses at $\vec{\mathbf{y}}_{q_0}$ with as less as energy as possible on the other points of the array $\{\vec{\mathbf{y}}_q, q \neq q_0\}$.

The analysis is straightforward as soon as we notice that, for a reflector at the position $\vec{\mathbf{y}}_{q_0}$, the imaging functional (9) at the search point $\vec{\mathbf{y}}_q$ can be written in the Fourier domain as

$$\hat{\mathcal{I}}_{\mathrm{IF}}(\vec{\mathbf{y}}_q, \vec{\mathbf{y}}_{q_0}, \omega) = \Big[(\mathcal{G}\hat{K}\mathcal{G}^\star)_{qq_0}\Big]^2 \overline{\hat{f}(\omega)}\,, \tag{B.2}$$

which is the square of the passive imaging functional (13) (without paying attention to the source term $\hat{f}(\omega)$). Therefore the optimization of the filter in the passive case performed in Section 3 also gives an efficient inverse filter in the active case.

Appendix C. Prolate spheroidal functions

We review some results that are taken from [17, 21] and that are relevant for our paper. The prolate spheroidal functions $\phi^n(x, C)$ are the eigenfunctions of the sinc kernel:

$$\int_{-1}^{1} \frac{\sin[C(x-y)]}{\pi(x-y)} \phi^n(y, C) dy = \eta^n(C)\phi^n(x, C)\,. \tag{C.1}$$

The symmetric kernel $\frac{\sin C(x-y)}{\pi(x-y)}$ is positive definite. Its spectrum $(\eta^n)_{n\geq 1}$ is discrete and positive, $\eta^1 > \eta^2 > \cdots > 0$ and $\eta^n \to 0$ as $n \to \infty$. The real-valued eigenfunctions ϕ^n are orthogonal on $(-1, 1)$ as well as on $(-\infty, \infty)$. They can be normalized so that

$$\int_{-\infty}^{\infty} \phi^n(x, C)\phi^m(x, C) dx = \mathbf{1}_m(n)\,, \tag{C.2}$$

and it then follows that

$$\int_{-1}^{1} \phi^n(x, C)\phi^m(x, C) dx = \eta^n(C)\mathbf{1}_m(n)\,. \tag{C.3}$$

By the spectral representation of the sinc kernel, we have

$$\sum_{n=1}^{\infty} \phi^n(x, C)\phi^n(y, C) = \frac{\sin[C(x-y)]}{\pi(x-y)} \quad \text{for } x, y \in (-1, 1)\,, \tag{C.4}$$

$$\sum_{n=1}^{\infty} \frac{1}{\eta^n(C)} \phi^n(x, C)\phi^n(y, C) = \delta(x-y) \quad \text{for } x, y \in (-1, 1)\,. \tag{C.5}$$

The eigenvalues $\eta^n(C)$ stay close to one for small n and then they plunge to 0 near the threshold value $[2C/\pi]$:

$$\eta^n(C) \overset{C\to\infty}{\longrightarrow} \begin{cases} 1 & \text{if } n = \left[\frac{2C}{\pi}(1-\epsilon)\right], \quad \epsilon > 0, \\ \frac{1}{1+e^{\pi b}} & \text{if } n = \left[\frac{2C}{\pi} + \frac{b}{\pi}\log C\right], \quad b \in \mathbb{R}, \\ 0 & \text{if } n = \left[\frac{2C}{\pi}(1+\epsilon)\right], \quad \epsilon > 0. \end{cases} \tag{C.6}$$

Finally, we have

$$\int_{-1}^{1} e^{-ixy}\phi^n(y, C) dy = \gamma^n(C)\phi^n\Big(\frac{x}{C}, C\Big), \qquad \gamma^n(C) = i^{n+1}\sqrt{\frac{2\pi\eta^n(C)}{C}}\,. \tag{C.7}$$

Appendix D. Discrete prolate spheroidal sequences

The discrete prolate spheroidal sequences are the eigenvalues of (28) in the case of a linear and regular array $\vec{\mathbf{x}}_r = (rh, 0, 0)$, $r = 1, \ldots, N$. We denote $w = h/\lambda$ and consider the case $w \leq 1/2$. These sequences are studied in detail in [20]. As pointed out in [2] they play a role in some inverse problems with discrete data. Using the relations (13) and (58) in [20], we find that the condition number of the matrix SI defined by (26) is of the form

$$C(w, N) \simeq \kappa(w) N^{-1/2} \exp(\gamma(w) N) \text{ as } N \to \infty\,, \tag{D.1}$$

with $\kappa(w) > 0$ and

$$\gamma(w) = \ln\Big(1 + \frac{2\sqrt{1+\cos(2\pi w)}}{\sqrt{2} - \sqrt{1+\cos(2\pi w)}}\Big)\,.$$

When $h \sim \lambda/2$, we have $w \sim 1/2$ and $\gamma(w) \sim 0$, the condition number of the matrix SI is not large.
When $h \ll \lambda$, we have $w \sim 0$ and $\gamma(w) \sim 4/(\pi^2 w^2)$, the condition number of the matrix SI is large.
This means that the matrix SI is well-conditioned when the array is sampled close to the Nyquist frequency, and ill-conditioned when the array is oversampled.

The number of eigenvalues significantly different from zero is approximately given by $2wN$ (this is the number of elements of an array whose diameter is Nh and which is sampled at the Nyquist rate).

References

[1] Bertero M and Boccaci P 1998 *Introduction to Inverse Problems in Imaging* (Bristol: Institute of Physics Publishing)

[2] Bertero M, De Mol C and Pike E R 1985 Linear inverse problems with discrete data. I. General formulation and singular system analysis *Inverse Problems* **1** 301-330

[3] Bertero M, De Mol C and Pike E R 1988 Linear inverse problems with discrete data: II. Stability and regularisation *Inverse Problems* **4** 573-594

[4] Biondi B L 2006 *3D Seismic Imaging* no. 14 in Investigations in Geophysics (Tulsa: Society of Exploration Geophysics)

[5] Blackstock D T 2000 *Fundamentals of Physical Acoustics* (New York: Wiley)

[6] Bleistein N, Cohen J K and Stockwell J W Jr 2001 *Mathematics of Multidimensional Seismic Imaging, Migration, and Inversion* (New York: Springer Verlag)

[7] Borcea L, Papanicolaou G, and Tsogka C 2006 Adaptive interferometric imaging in clutter and optimal illumination *Inverse Problems* **22** 1405-1436

[8] Borcea L, Papanicolaou G, and Tsogka C 2007 Optimal waveform design for array imaging *Inverse Problems* **23** 1973-2021

[9] Born M and Wolf E 1999 *Principles of Optics* (Cambridge: Cambridge University Press)

[10] Chan T F and Shen J 2005 *Image Processing and Analysis: Variational, PDE, Wavelet, and Stochastic Methods* (Philadelphia: SIAM)

[11] Claerbout J F 1985 *Imaging the Earth's Interior* (Palo Alto: Blackwell Scientific Publications)

[12] Craven P and Wahba G 1979 Smoothing noisy data with spline functions: estimating the correct degree of smoothing by the method of GCV *Numer. Math.* **31** 377-403

[13] Dorn O 2004 Time-reversal and the adjoint method with an application in telecommunication arXiv:math.OC/0412379v1

[14] Fink M 1992 Time reversal of ultrasonic fields - Part I: Basic principles *IEEE Trans. Ultrason. Ferroelectr. Freq. Control* **39** 555-566

[15] Golub G, Heath M and Wahba G 1979 Generalized cross-validation as a method for choosing a good ridge parameter *Technometrics* **21** 215-223

[16] Haddadin O and Ebbini E 1998 Ultrasonic focusing through inhomogeneous media by application of the inverse scattering problem *J. Acoust. Soc. Am.* **104** 313-325

[17] Landau H J and Widom H 1980 The eigenvalue distribution of time and frequency limiting *J. Math. Anal. Appl.* **77** 469-481

[18] Priestley M B 1981 *Spectral Analysis and Time Series* (London: Academic Press)

[19] Rhodes D R 1963 The optimum line source for the best mean-square approximation to a given radiation pattern *IEEE Transactions on Antennas and Propagation* **AP-11** 440-446

[20] Slepian D 1978 Prolate spheroidal wavefunctions, Fourier analysis, and uncertainty - V: The discrete case *Bell Syst. Tech. J.* **57** 1371-1429

[21] Slepian D 1983 Some comments on Fourier analysis, uncertainty and modeling *SIAM Review* **25** 379-393

[22] Tanter M, Aubry J F, Gerber J, Thomas J L and Fink M 2001 Optimal focusing by spatio temporal inverse filter. I. Basic principles *J. Acoust. Soc. Am.* **110** 37-47

[23] Tanter M, Thomas J L and Fink M 2000 Time reversal and the inverse filter *J. Acoust. Soc. Am.* **108** 223-234

[24] Taylor T T 1955 Design of line-source antennas for narrow beamwidths and low sidelobes *IRE Trans. Antennas Propag.* **AP-3** 16-22

[25] Tikhonov A N 1963 Solution of incorrectly formulated problems and the regularization method *Sov. Math. Dokl.* **4** 1035-1038

[26] Twomey S 1985 The application of numerical filtering to the solution of integral equations encountered in indirect sensing measurements *J. Franklin Inst.* **279** 95-109

[27] Vignon F, de Rosny J, Aubry J F and Fink M 2007 Optimal adaptive focusing through heterogeneous media with the minimally invasive inverse filter *J. Acoust. Soc. Am.* **122** 2715-2724

[28] Vogel C R 2002 *Computational Methods for Inverse Problems* (Philadelphia: SIAM Frontiers in Applied Mathematics)

[29] Wapenaar K and Fokkema J 2006 Green's function representations for seismic interferometry *Geophysics* **71** SI33-SI46